Coseismic deformation of the 2001 Mw = 7.8 Kokoxili earthquake in Tibet, measured by synthetic aperture radar interferometry

Cécile Lasserre, G. Peltzer, F. Crampé, Yann Klinger, Jerome van Der Woerd, Paul Tapponnier

Coseismic deformation of the 2001 M_w = 7.8 Kokoxili earthquake in Tibet, measured by synthetic aperture radar interferometry

C. Lasserre,[1,2] G. Peltzer,[1,3] F. Crampé,[1] Y. Klinger,[4] J. Van der Woerd,[5] and P. Tapponnier[4]

Received 25 October 2004; revised 5 October 2005; accepted 19 October 2005; published 23 December 2005.

[1] The 14 November 2001, M_w = 7.8, Kokoxili earthquake ruptured more than 400 km of the westernmost stretch of the left-lateral Kunlun fault in northern Tibet. Interferometric synthetic aperture radar data from descending orbits, along four adjacent tracks covering almost the entire rupture, and 1-m pixel Ikonos satellite images are used to map the rupture geometry and the surface displacements produced by the event. Interferograms are then inverted to solve for coseismic slip on the fault at depth. The radar data show that the rupture connected the Heituo fault, where the earthquake initiated, to the main Kunlun fault, cutting across a pull-apart trough in between the two strike-slip faults. The fault model includes two vertical sections extending to a depth of 20 km and discretized into 5 km × 5 km patches. Using a nonnegative least squares method that includes an appropriate degree of smoothing, we solve for the left-lateral slip on each fault patch. Our solution shows that the largest slip occurred at depths between 0 and 5 km, reaching ≃8 m in two areas, 200 and 250 km east of the earthquake epicenter. Significant slip took place below 10 km at both ends of the rupture. Slip appears to have been highly variable along the fault, defining six sections of major moment release. These sections correspond to six subsegments of the Kunlun fault system, defined from the surface morphology of the fault. This suggests that fault geometry exerted a predominant influence on controlling the rupture propagation.

Citation: Lasserre, C., G. Peltzer, F. Crampé, Y. Klinger, J. Van der Woerd, and P. Tapponnier (2005), Coseismic deformation of the 2001 M_w = 7.8 Kokoxili earthquake in Tibet, measured by synthetic aperture radar interferometry, *J. Geophys. Res.*, *110*, B12408, doi:10.1029/2004JB003500.

1. Introduction

[2] On 14 November 2001, a M_w = 7.8 earthquake ruptured more than 400 km of the westernmost part of the Kunlun fault [*Xu et al.*, 2002; *Van der Woerd et al.*, 2002a], a major left-lateral strike-slip fault of northern Tibet in Qinghai province [e.g., *Tapponnier and Molnar*, 1977; *Van der Woerd et al.*, 2000, 2002b]. This earthquake (named the Kokoxili earthquake) is the largest event to have occurred in China in the past fifty years. It was preceded four years earlier by a M_w = 7.6 event (8 November 1997) that ruptured the left-lateral Manyi fault over a length of 170 km, about 250 km to the southwest [*Peltzer et al.*, 1999; *Velasco et al.*, 2000] (Figure 1a).

[3] The epicenter of the Kokoxili earthquake determined by the U.S. Geological Survey (USGS) National Earthquake Information Center (NEIC) is located at 35.95°N and 90.54°E, southwest of the Buka Daban Feng range, off the main Kunlun fault (Figure 1b). The rupture initiated west of Taiyang lake, on a secondary strike-slip fault within the complex horsetail system that forms the western end of the Kunlun fault (Figure 1b). It then propagated eastward, breaking through a 45-km-long and 10-km-wide pull-apart trough, to merge with the main trace of the Kunlun fault east of 91°E. East of 93.75°E, the rupture continued on the Kunlun Pass fault along the southern front of the Burhan Budai Shan, ending near 95°E [*Xu et al.*, 2002; *Van der Woerd et al.*, 2002a] (Figure 1b). In a preliminary field study, *Lin et al.* [2002] reported a maximum horizontal coseismic slip of 16 m, east of Kusai lake, at 93.3°E, close to the centroid location (Harvard centroid moment tensor (CMT) catalog, Figure 1b). Later field measurements of along-strike variations of slip [*Xu et al.*, 2002; *Van der Woerd et al.*, 2003], and the analysis of high-resolution satellite images (Ikonos and Quick Bird, [*Klinger et al.*, 2005]) acquired after the earthquake concur to indicate

[1]Department of Earth and Space Sciences, University of California, Los Angeles, California, USA.
[2]Now at Laboratoire de Géologie, École Normale Supérieure, CNRS-UMR 8538, Paris, France.
[3]Also at Jet Propulsion Laboratory, California Institute of Technology, Pasadena, California, USA.
[4]Laboratoire de Tectonique et Mécanique de la Lithosphère, Institut de Physique du Globe de Paris, Paris, France.
[5]Institut de Physique du Globe de Strasbourg, CNRS-UMR 7516, Strasbourg, France.

0148-0227/05/2004JB003500$09.00

smaller values of the maximum horizontal slip, ranging between 7.5 to 10 m, at similar longitudes. The vertical offsets along the rupture were small, mostly below 1 m. Normal throws were observed within the extensional step-over at the western end of the rupture [*Klinger et al.*, 2005]. Vertical motion was also observed along a 50-km-long normal fault following the range front, northwest of Kusai lake, associated with slip partitioning [*Van der Woerd et al.*, 2002a; *Bowman et al.*, 2003; *King et al.*, 2005; *Klinger et al.*, 2005].

[4] Models of the rupture process from body and surface wave inversion suggest that rupture along the Kusai Hu segment of the Kunlun fault propagated continuously and unilaterally eastward, at supershear velocity [*Bouchon and Vallée*, 2003; *Vallée et al.*, 2003; *Antolik et al.*, 2004]. The rupture mechanism is mainly left-lateral strike slip [e.g., *Rivera et al.*, 2003]. However, *Antolik et al.* [2004] propose that two subevents occurred in the first 18 s of the rupture, preceding the main moment release along the Kunlun fault. They suggest that the rupture initiated with a $M \simeq 6.8$ strike-slip event, along the strike-slip segment west of Taiyang lake, followed 5 s later by an oblique-normal event of similar magnitude, likely along the 45-km-long, extensional step-over northeast of the lake (Figure 1b). To the east, the rupture transferred to the main Kunlun fault, and propagated 350 km farther, with a maximum slip of 7.5 m occurring 200 to 250 km east of the epicenter [*Antolik et al.*, 2004].

[5] Field observations and seismological studies provide a broad picture of the earthquake rupture. However, the length of the rupture, among the longest ever observed for a strike-slip event, its complexity, and the remoteness of the area made it difficult to construct a complete map of the coseismic displacements at the surface from field measurements only. In some areas, the width of the rupture zone reaches several hundreds of meters, involving multiple parallel strands, slip partitioning, and extensional or compressional structures at various scales [*Xu et al.*, 2002; *Van der Woerd et al.*, 2003; *Li et al.*, 2005], leading to uncertainties in the measurements. Coseismic slip distribution models derived from inversion of seismological data highlight only the main segments with large slip amounts along the rupture. GPS data collected before the earthquake are too sparse to constrain variable slip solutions [*Wang et al.*, 2003]. Deployment of GPS instruments after the event is being used to measure postseismic deformation, mainly along the eastern part of the rupture [*Freymueller and Wang*, 2003; *Shen et al.*, 2003].

[6] Synthetic aperture radar interferometry (InSAR) provides the mean to study the overall coseismic deformation associated with the Kokoxili earthquake. In this paper, we use ERS InSAR data from descending orbits, along four adjacent tracks covering almost the entire rupture, the 3-arc sec Shuttle Radar Topography Mission (SRTM) digital elevation model [*Farr and Kobrick*, 2000], and 1-m pixel Ikonos images. We first determine the rupture geometry and map the surface displacements produced by the event. In particular, we explore the rupture within the Buka Daban Feng pull-apart in the west, a long slip transfer zone between two strike-slip segments, which is of particular interest in understanding rupture dynamics [e.g., *Harris and Day*, 1993]. The analysis of Ikonos images is fully developed by *Klinger et al.* [2005], providing a detailed description of surface deformation and rupture style over the $\simeq$200-km-long, eastern part of the 2001 break. This paper focuses on InSAR data, used to derive a variable strike-slip model for the Kokoxili event. Our slip distribution model provides new insights into the rupture mechanism. It suggests that the 2001 break extends to a depth of $\simeq$20 km, with most slip occurring within the upper 10 km, and includes six distinct sections of moment release. These sections correspond to fault subsegments that are independently defined from the surface morphology of the fault.

2. Seismotectonic Setting

[7] The Kunlun fault is one of the principal left-lateral strike-slip fault systems that slice the northern part of the tibetan plateau (Figure 1a). It runs for about 1600 km from 86°E to 105°E, striking N100–N110°E on average. It accommodates the eastward movement of the Qiangtang and Songpan blocks of Tibet with respect to the Qaidam basin [*Kidd and Molnar*, 1988; *Tapponnier et al.*, 2001]. East of 91°E, the Kunlun fault follows the southern front of the Kunlun range, and can be divided into six main segments [*Van der Woerd et al.*, 2000, 2002b] (Figure 1a). West of 91°E, the fault splays into a complex horsetail system, including in the south the $\simeq$250-km-long Manyi left-lateral fault [*Tapponnier and Molnar*, 1977] (Figure 1a). The long-term, millennial slip rate along most of the Kunlun fault has

Figure 1. (a) Simplified map of Kunlun fault system. Six segments defined by *Van der Woerd et al.* [2002b] along main Kunlun fault (labeled A to F) are indicated with dashed blue vertical lines. Surface ruptures associated with 1997, $M_w = 7.6$, Manyi and 2001, $M_w = 7.8$, Kokoxili earthquakes are outlined in blue and red, respectively. Corresponding CMT focal mechanisms are in similar color. The 1937, $M = 7.5$, historical earthquake (in red [*Gu et al.*, 1989]) and $M_s > 4$ instrumental seismicity (open circles) along fault are also reported. Corresponding focal mechanisms are from *Molnar and Lyon-Caen* [1989] and USGS. Note widening of the Kunlun fault zone in a horsetail system west of the Kusai Hu segment. Inset map shows location of Kunlun fault (in red) within India-Asia collision zone. Light and dark grey boxes indicate map coverage of Figures 1a and 1b, respectively. (b) Seismotectonic map of western Kunlun fault system. The 2001 Kokoxili earthquake rupture is outlined in red. Gray and yellow circles are $M \geq 5$ events prior to the earthquake (27 March 1998 to 13 November 2001) and aftershocks (14 November 2001 to 31 December 2003), respectively. The main shock is shown in red. Locations are from Advanced National Seismic System (ANSS) catalog. Focal mechanisms from Harvard CMT catalog are plotted in similar shades and point to locations from ANSS catalog (large circles) and CMT centroids (small circles). Topography is from 3-arc sec Shuttle Topography Mission (SRTM) digital elevation data. BDF and BBS refer to Buka Daban Feng and Burhan Budai Shan summits, respectively. Black rectangles outline the location of interferograms shown in Figure 2. See color version of this figure at back of this issue.

been estimated to be 11.5 ± 2 mm/yr, from surface dating of geomorphic markers offset by the fault [*Van der Woerd et al.*, 1998, 2000, 2002b; *Li et al.*, 2005]. This rate is compatible with the decadal slip rate (≃1 cm/yr), derived from GPS measurements [*Wang et al.*, 2001].

[8] In the last 100 years, the Kunlun fault system generated five $M \geq 7$ earthquakes, including the most recent 2001 Kokoxili event along the Kusai Hu segment (Figure 1a) [*Gu et al.*, 1989]. In 1937, the $M \simeq 7.5$ Dongxi Co earthquake (epicenter near longitude 97.5°E [*Jia et al.*, 1988]) produced a 150-km-long break with left-lateral slip of up to 7 m [*Li and Jia*, 1981]. It was followed in 1963 by a M_w = 7.1 sinistral event, about 100 km farther west [*Fitch*, 1970] (Figure 1a). The westernmost strand of the Kunlun fault

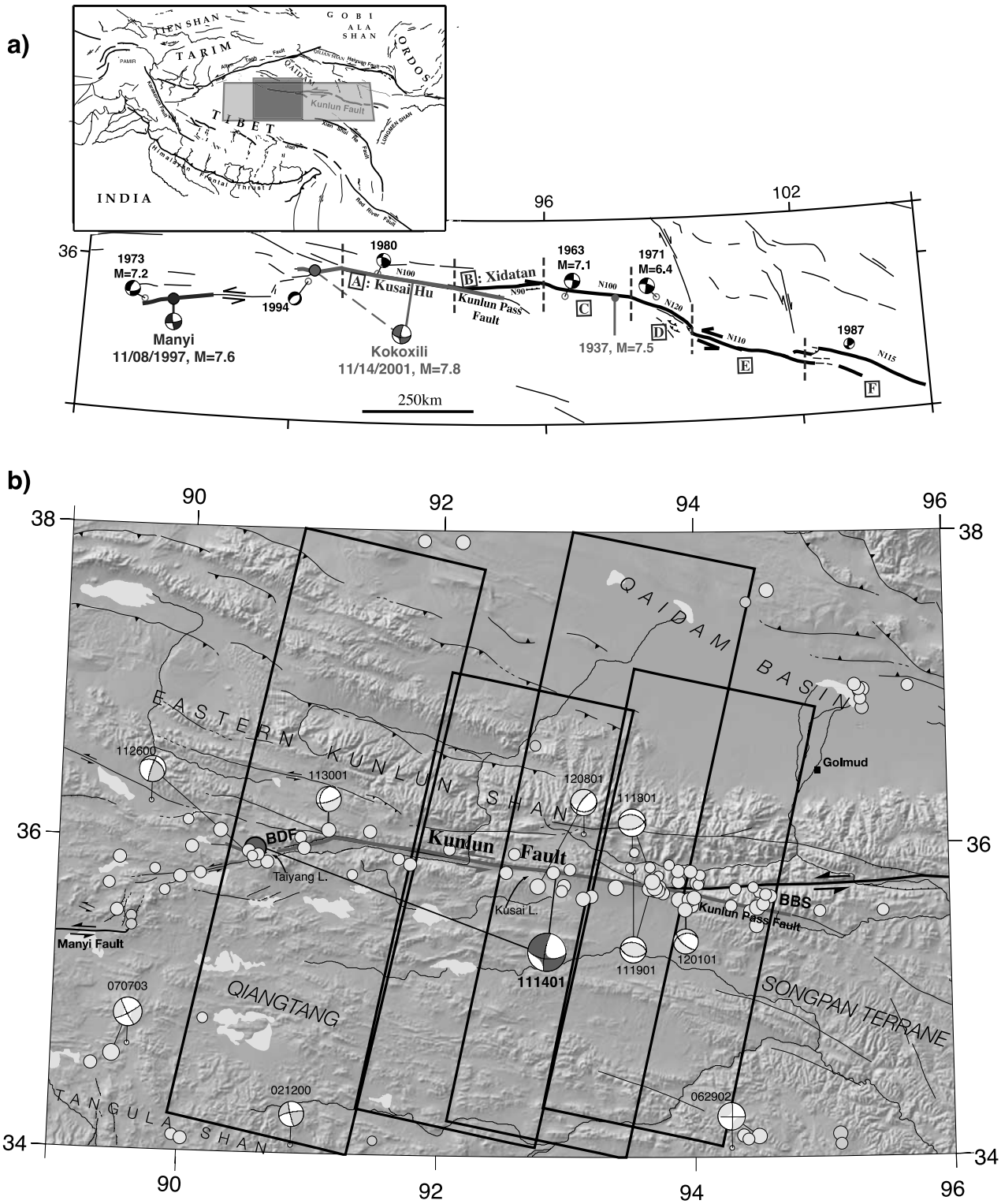

Figure 1

Table 1. Summary of Processed ERS Interferograms[a]

Track	Frames	Scene 1 Satellite-Orbit (Date)	Scene 2 Satellite-Orbit (Date)	T, years	$B_\perp$, m
448	**2853/2871/2889/2907**	**ERS2-15332 (26 Mar 1998)**	**ERS2-36875 (9 May 2002)**	**4.1**	**15**
405	**2871/2889/2907**	**ERS1-37467 (13 Sep 1998)**	**ERS2-35329 (22 Jan 2002)**	**3.3**	**60**
405	2871/2889[b]/2907	ERS2-28816 (23 Oct 2000)	ERS2-34828 (17 Dec 2001)	1.1	13
405	2871/2889	ERS2-32323 (25 Jun 2001)	ERS2-34828 (17 Dec 2001)	0.5	242[c]
133	**2853/2871/2889/2907**	**ERS2-21029 (28 Apr 1999)**	**ERS2-35057 (2 Jan 2002)**	**2.7**	**63**
133	2871/2889/2907	ERS2-17021 (22 Jul 1998)	ERS2-35057 (2 Jan 2002)	3.5[d]	50
133	2871/2889	ERS2-9506 (12 Feb 1997)	ERS2-35057 (2 Jan 2002)	4.9[d]	50
362	**2871/2889/2907**	**ERS2-33783 (5 Oct 2001)**	**ERS2-34785 (14 Dec 2001)**	**0.2**	**15**

[a]Only data from descending orbits were available. $B_\perp$ represents perpendicular baseline at top of each track. T refers to temporal baseline. The Kokoxili earthquake occurred on 14 November 2001. Bold indicates selected data for inversion of fault slip distribution.
[b]Missing data in the fault zone.
[c]Longer baseline than selected pair.
[d]Longer time span than selected pair.

system ruptured in 1973 (M_w = 7.2 oblique normal slip event), then in 1997 during the M_w = 7.6 Manyi event, producing a 170-km-long sinistral rupture with up to 7 m of slip [*Peltzer et al.*, 1999]. Two $M \simeq 5.5$ events occurred north of (in 1980) or west of (in 1994) the N100 striking, $\simeq$270-km-long, Kusai Hu segment of the Kunlun fault, prior to the Kokoxili earthquake (Figure 1a). The 1994 earthquake, located about 10 km south of the Kokoxili earthquake epicenter, has a NE striking nodal plane with a normal component of slip, compatible with the SW-NE trending normal faults observed in this area [*Van der Woerd et al.*, 2002b].

3. Analysis of ERS InSAR Data

[9] To map the Kokoxili earthquake displacement field, we used SAR images acquired before and after the event by the European Space Agency's ERS satellites. Only radar scenes from descending orbits were available. The failure of an attitude control device of the ERS2 satellite occurred 10 months before the 14 November 2001 Kokoxili earthquake, limiting the number of ERS image pairs that could be combined into interferograms. InSAR data from four adjacent tracks cover almost the entire rupture length, except for a few kilometers at both its western and eastern ends (Figure 1b and Table 1). All available data were processed and, for the present study, only one interferogram was selected on each track based on the level of coherence throughout the scene (Figure 2).

[10] Raw SAR data were processed into interferograms averaged at four looks using the Jet Propulsion Laboratory, California Institute of Technology, repeat orbit interferometry package ROI_PAC [*Rosen et al.*, 2004]. We used the restituted orbits of the ERS spacecrafts provided by European Space Agency. The topographic component of the interferometric phase was removed using the 3-arc sec SRTM data. The phase unwrapping was done independently for each side of the fault. Because of low coherence in the mountain and swamp areas, particularly south of the fault, some patches of coherent phase remained disconnected from one another in the wrapped interferograms. The phase ambiguity (number of cycles of 2π) between nearby patches belonging to the same side of the fault was estimated visually to construct the unwrapped phase field over the image (Figure 2). This was done by inspecting phase profiles connecting nearby, disconnected patches in the interferogram. The process was initiated in areas of good phase coherence, near the fault, progressing toward the far field in areas of lower coherence and lower phase variability (see profiles in Figures 3a–3c). Patches for which the number of phase cycles could not be determined within one cycle due to the phase noise were dropped in the process. Finally, the phase constant between the north and south sides of the fault was estimated along with the slip solution in the inversion.

[11] Figure 2 shows the line of sight (LOS) component of the surface displacement produced by the earthquake. The selected interferograms span time intervals of various durations starting from 3.7 years to 1 month before the earthquake and ending between 1 month and 6 months after it (Figure 2 and Table 1). The phase observed in each interferogram thus contains interseimic and postseismic deformation signal in variable amounts. Time intervals covered by interferograms increase from east to west, ranging from 2 months on track 362 (T362) to 4.1 years on track 448 (T448). This results in an increasing loss of phase coherence from east to west (Figure 2). At such high elevation (above 4500 m above sea level), temporal decorrelation is probably caused by seasonal snow cover on the high summits as well as freeze thaw cycles producing changes in the scattering properties of the surface [*Rosen et al.*, 2000; *Zebker and Villasenor*, 1992]. In the vicinity of the rupture zone, the observed decorrelation may be due to high strain and ground disruption related to the earthquake, as commonly reported in InSAR studies of earthquakes [e.g., *Massonnet et al.*, 1993; *Zebker et al.*, 1994; *Peltzer et al.*, 1999].

[12] Despite the important decorrelation on the westernmost interferograms, the InSAR data provide spatially dense information on the extent and style of the rupture. The large-scale fringe pattern is consistent with left-lateral displacement on the fault (Figure 2). Smaller-scale, elliptical patterns of fringes observed along the fault in wrapped and unwrapped interferograms indicate high variability of the shallow slip along the fault. In the following sections, we examine the interferometric phase near the western and eastern ends of the rupture.

3.1. Western End of the Rupture

[13] The 4-year spanning T448 interferogram shows disconnected patches of unwrapped phase that make identification of the surface rupture difficult in the epicentral

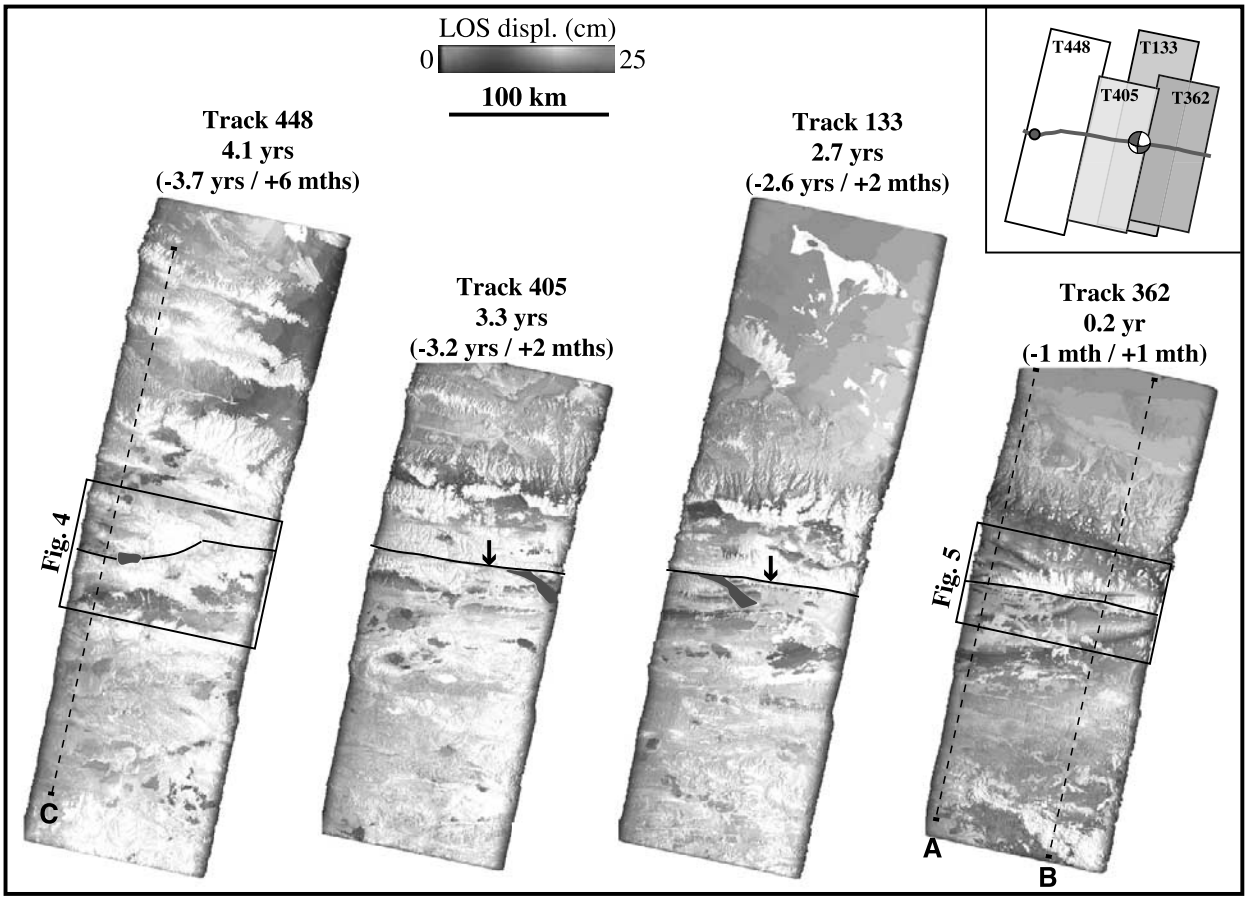

Figure 2. Interferograms showing coseismic surface displacement associated with 14 November 2001 Kokoxili earthquake. One color cycle (blue-red-yellow) represents 25 cm of ground displacement toward the satellite along radar line of sight. Grey areas are zones of low coherence that have been masked for phase unwrapping. Inset box shows locations of rupture, USGS NEIC epicenter and Harvard CMT centroid in interferograms. Time interval covered by each interferogram is indicated, with fractions of interval before and after the earthquake in parentheses (see also Table 1). Solid black line is simplified rupture trace used for modeling. Dashed lines indicate locations of profiles in Figures 3a–3c. Arrows point to location of Ikonos images shown in Figure 6. Boxes on tracks 448 and 362 indicate areas covered by Figures 4 and 5, respectively. See color version of this figure at back of this issue.

area of the earthquake (Figure 2). The shape of the fringes in the wrapped phase image helps us assessing the rupture location in this area (Figure 4).

[14] Figure 4a shows the active faults in this western region of the Kunlun fault system, mapped independently from the analysis of fault morphology on satellite images, and superimposed on the SAR amplitude image of this area. The main active structure is a 45-km-long, 10-km-wide pull-apart trough south of Buka Daban Feng, connecting the Kunlun fault with the Heituo fault, a strike-slip segment along the northern front of Heituo Feng, west of Taiyang lake. The wrapped interferogram shows that the Heituo fault bounds to the south a half-lobe pattern of dense fringes (Figure 4b). Such a pattern is characteristic of the surface strain observed against faults near the termination of an earthquake rupture [e.g., *Massonnet et al.*, 1993], indicating that the 2001 surface break followed the Heituo fault. This is consistent with field observations of a 26-km-long, N105 striking surface rupture along this fault [*Xu et al.*, 2002; *Klinger et al.*, 2005]. East of Taiyang lake, we located the rupture along the northern edge of coherent patches of phase where similar patterns of fringes can be observed (Figure 4b). This rupture does not follow the main Quaternary fault traces mapped from satellite images along either side of the Buka Daban Feng pull-apart basin, but cuts across it. Discontinuous 2001 surface breaks were mapped in the field along scarps following the northern side of the pull-apart [*Klinger et al.*, 2005], in areas where the phase is incoherent in the interferogram (Figure 4). They do not coincide either with the rupture derived from the phase image. It is possible that the rupture zone most consistent with the phase image was missed in the field because located along swamps, streams or glacial outwash. In fact, the $\simeq$70-km-long lobe of fringes that surrounds the Taiyang lake on the south side suggests that the rupture was continuous at depth between the Heituo fault and the main Kunlun fault, with complexities occurring near the junction with the latter. Such continuity of the rupture was also suggested by seismological models [*Antolik et al.*, 2004].

[15] In the model below, we take the entire $\simeq$90-km-long, curved fault southwest of the main Kunlun fault (Figure 4b) to be the main fault that broke within the horsetail system

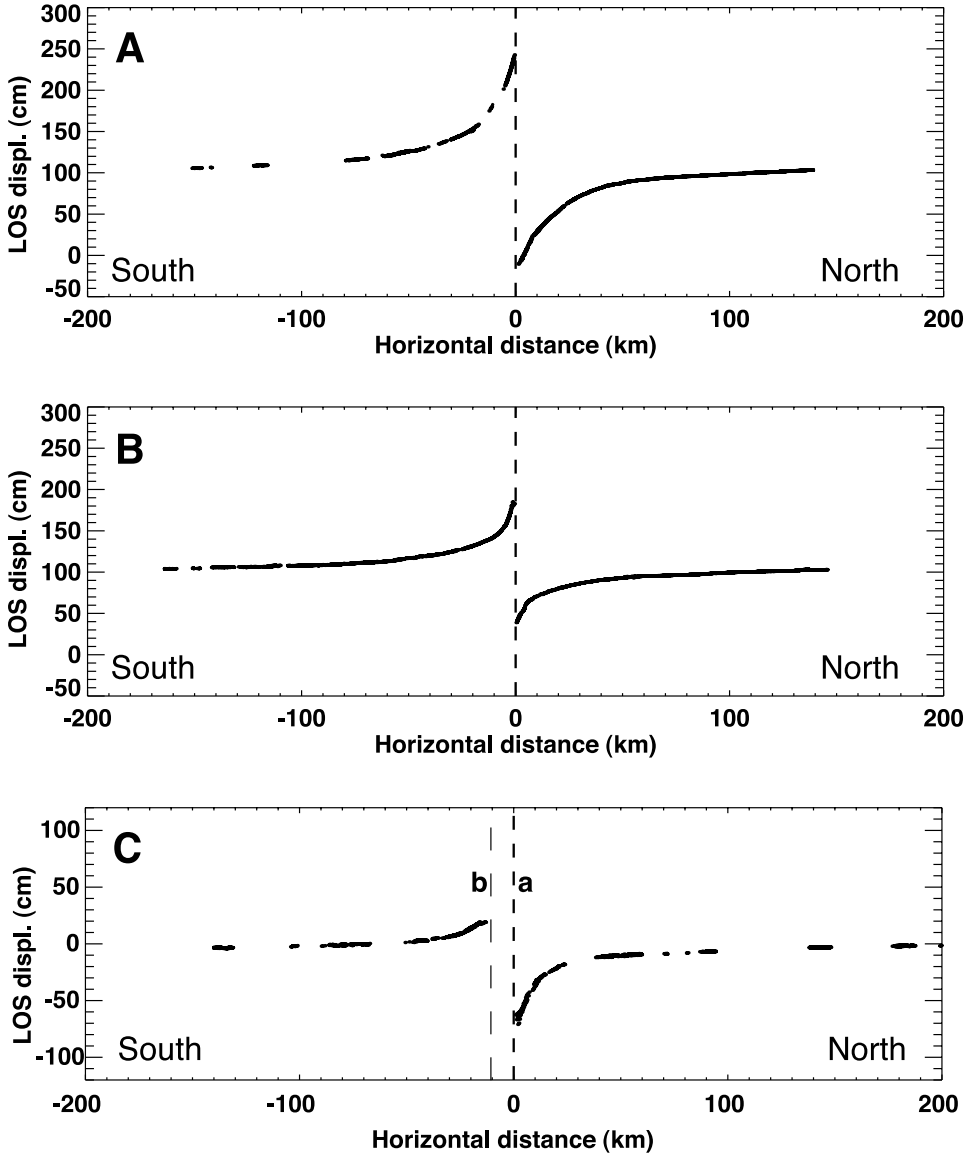

Figure 3. Observed LOS displacement profiles (see location in Figure 2) across (a) Kunlun fault east of Kusai lake (profile A), (b) Kunlun Pass fault (profile B), and (c) Heituo fault west of Taiyang lake (profile C). Profile A intersects with fault close to area where maximum displacement was measured in the field [*Xu et al.*, 2002]. Origin of distance on horizontal axis is at main surface break. Labels a and b on profile C indicate locations of faults discussed in text and shown in Figure 4b.

during the 2001 earthquake. This fault is referred to as the Taiyang lake fault in the following. Secondary slip along other faults south of the Heituo Feng range and along the Buka Daban Feng pull-apart may have occurred (thin white dashed lines on Figure 4b) but is not included in the modeling. The north-south LOS displacement profile across faults west of Taiyang lake (Figures 3c and 4b) shows a larger displacement gradient north of Heituo Feng than south of it. This confirms that coseismic slip occurred mainly along the Heituo fault, which bounds the range's north side, but not along faults south of the range.

3.2. Eastern End of the Rupture

[16] Interferogram T362 shows two main lobes in the pattern of fringes surrounding the fault (Figure 2). The western lobe defines a $\simeq$70-km-long subsegment along the eastern end of the Kusai Hu segment of the Kunlun fault. It closes to the east near the junction between this segment and the Kunlun Pass fault (Figure 5). It is centered on the fault stretch where the largest left-lateral slip has been reported. Horizontal offsets of 7.6 m were observed in the field [*Xu et al.*, 2002] and up to 9 m of left-lateral slip was measured on Ikonos images [*Klinger et al.*, 2005], near 93°2*E*. A displacement profile from InSAR data across this segment of the fault, about 15 km west of the maximum slip area, indicates $\simeq$2.7 m of LOS offset between the two sides of the fault (Figures 2 and 3a). This value projects into $\simeq$7 m of left-lateral slip if we assume purely horizontal movement parallel to the fault. Measurement from various data sources thus concur to a maximum slip of about 8 m.

[17] The second lobe of fringes observed in the eastern part of interferogram T362 surrounds the 50-km-long seg-

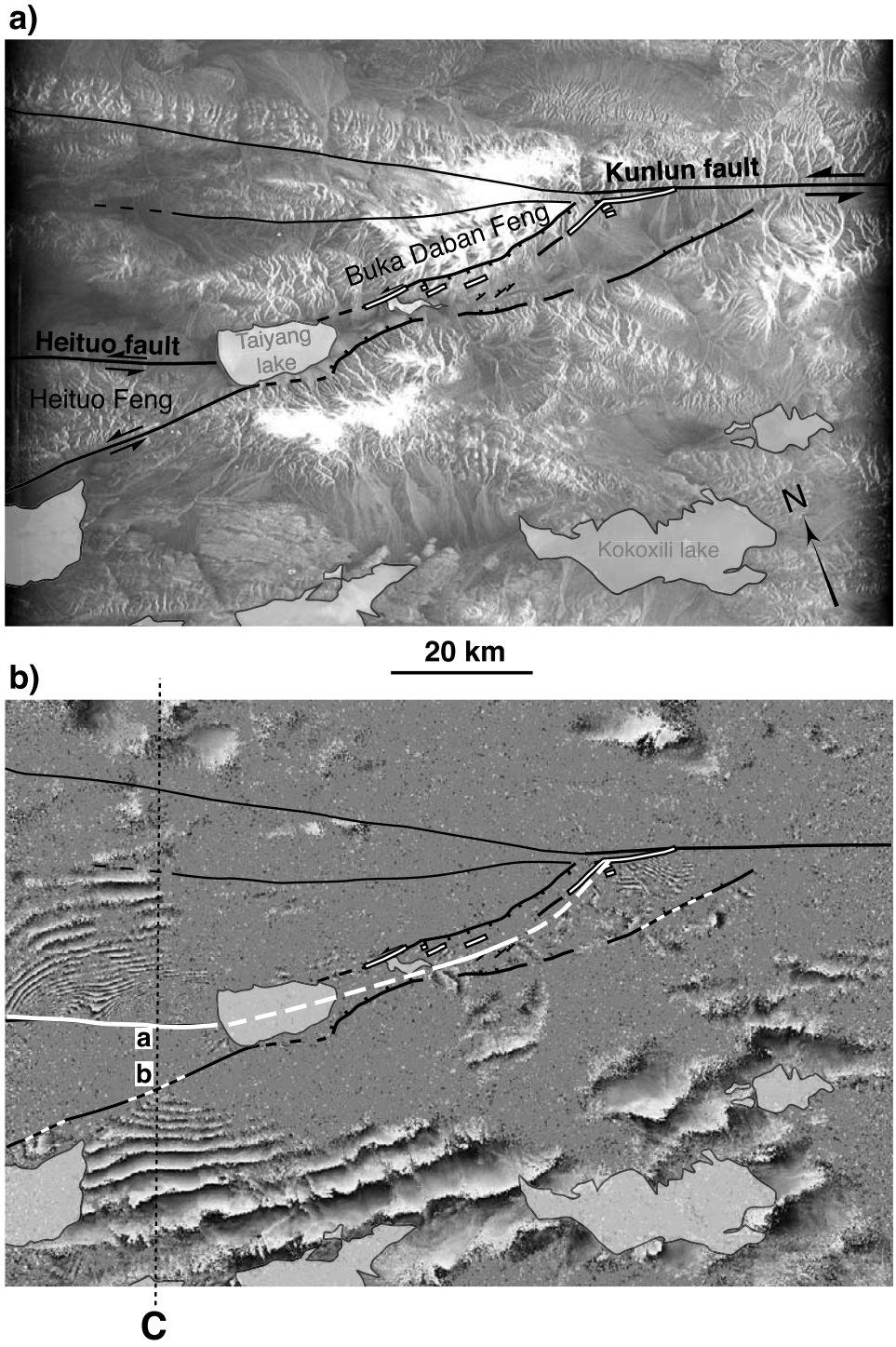

Figure 4. (a) Radar amplitude image of western part of rupture zone (see location in Figure 2). Black lines are active faults. Faults with normal component of movement are shown with ticks on hanging wall side. A 45-km-long, 10-km-wide pull-apart marks western end of Kunlun fault, east of Taiyang lake. White filled black lines indicate surface ruptures observed there in the field by *Klinger et al.* [2005]. (b) Wrapped interferometric phase over same area as in Figure 4a. One grey cycle represents 2.8 cm of LOS displacement. Zones with incoherent phase have been masked for clarity. Active faults and surface ruptures from Figure 4a are reported. Thick white lines outline rupture trace used to construct fault model southwest of main Kunlun fault, well defined (solid lines) or inferred (dashed lines) from fringe pattern (see text). Thin, white dashed lines follow other plausible ruptured segments, ignored in modeling. Black dotted line shows location of profile C in Figure 3. Labels a and b refer to faults location on profile.

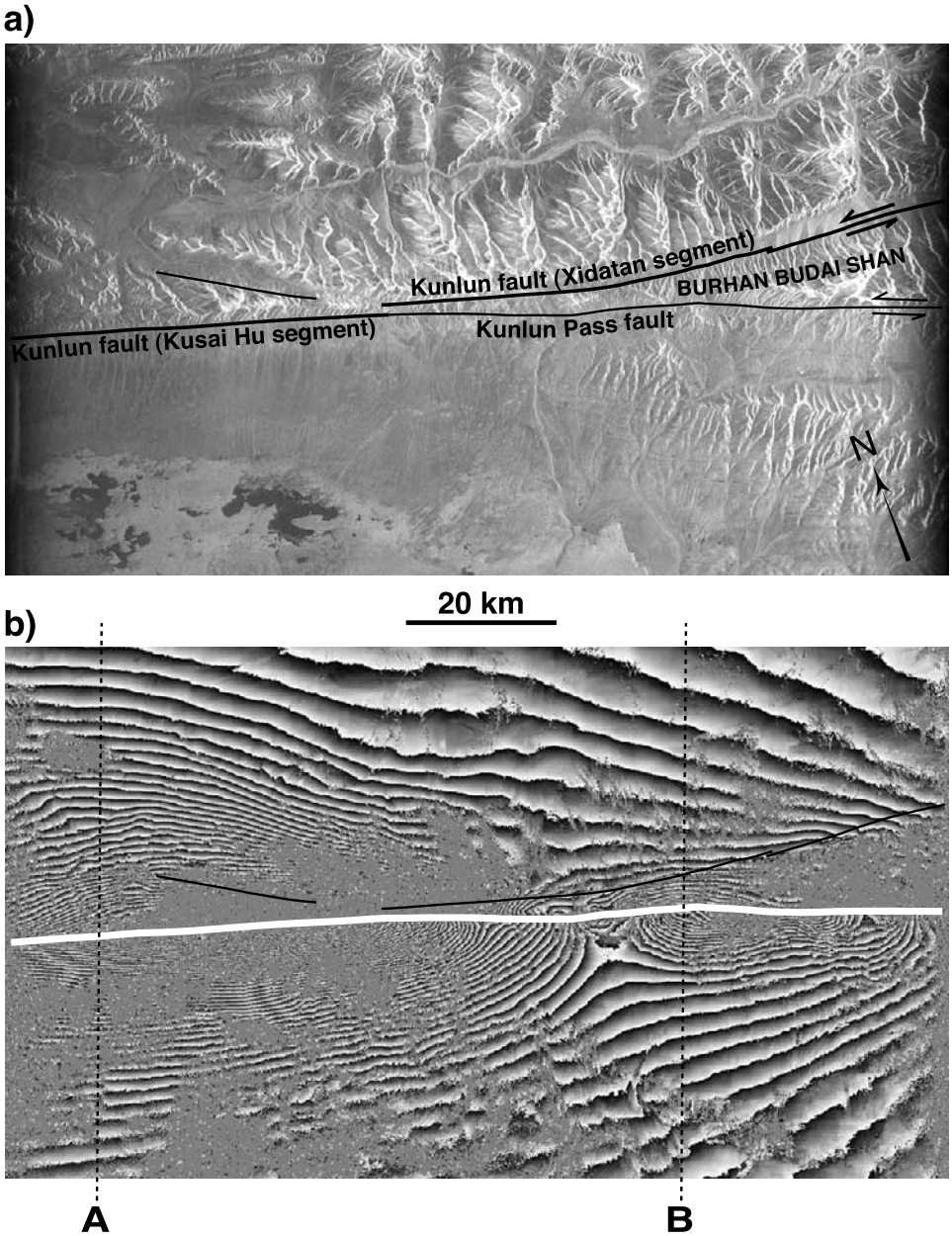

Figure 5. (a) Radar amplitude image covering eastern end of rupture (see location in Figure 2). Solid lines are active faults from *Van der Woerd et al.* [2002b] and Ikonos images analysis (this study). (b) Wrapped interferometric phase over same area as in Figure 5a. One grey cycle represents 2.8 cm of LOS displacement. Zones with incoherent phase have been masked for clarity. Faults from Figure 5a are depicted in black. Solid white line outlines rupture trace inferred from analysis of Ikonos images, consistent with fringe pattern. Black dotted lines shows location of profiles A and B in Figure 3.

ment of the Kunlun Pass fault at the end of which the eastward propagating 2001 rupture stopped (Figure 5). A LOS displacement profile across this segment indicates a maximum horizontal slip of about 4 m, assuming pure strike slip (Figures 2 and 3b), in good agreement with field measurements [*Xu et al.*, 2002].

[18] Small size complexities in the pattern of fringes are observed in the area where the Xidatan segment of the Kunlun fault and the Kunlun Pass fault run parallel, less than 10 km apart, before splaying on both sides of the Burhan Budai range (Figure 5). They attest to local variations in the shallow slip and can be related to local changes in the fault strike, precisely mapped from Ikonos images, and in the fault dip. The fringes go undeviated across the Xidatan segment of the Kunlun fault, indicating that this segment did not rupture during the earthquake.

4. Modeling Fault Slip Distribution

[19] Inverse modeling of InSAR data to solve for slip distribution along the fault plane requires a priori knowledge of the fault geometry (fault orientation, dip and depth). The fault model used in this study is based on our own mapping of the rupture using InSAR wrapped phase images

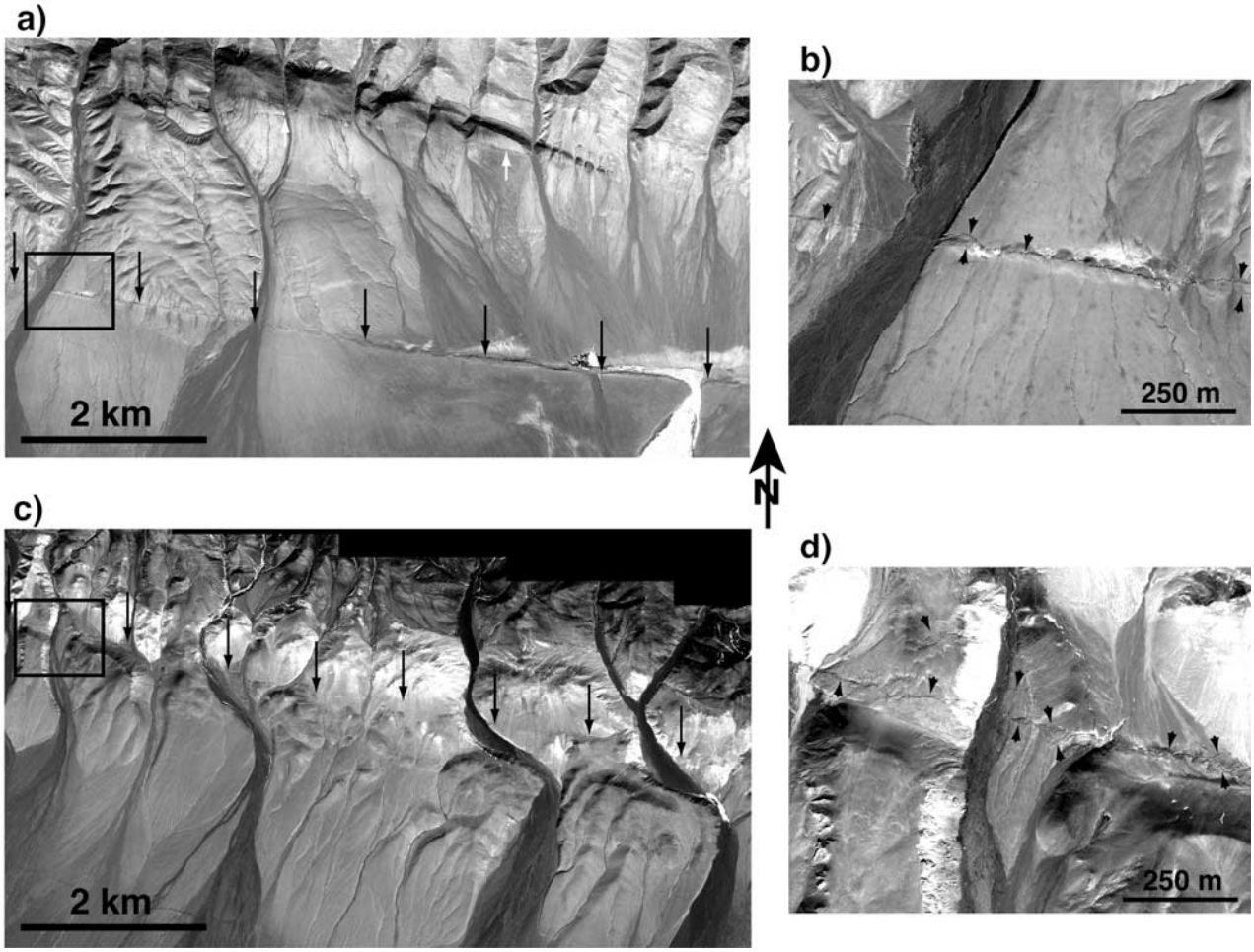

Figure 6. The 1-m pixel Ikonos satellite images showing surface ruptures associated with 2001 Kokoxili earthquake. (a) Rupture trace west of Kusai lake near longitude 92.2°E (see location in Figure 2). Black arrows point to linear surface rupture across alluvial fans, following cumulative, north facing scarp in eastern part of image. White arrows point to normal fault scarps along mountain front, along which 2001 rupture was discontinuous. Box indicates location of Figure 6b. (b) Push-up structures disrupted by 2001 breaks. (c) Rupture trace at southern front of mountain range, east of Kusai lake (see location in Figure 2). Note en echelon steps along rupture. Kilometric offsets of rivers correspond to cumulative slip on fault. Box shows location of Figure 6d. (d) Detail of Figure 6c illustrating rupture complexities. Note multiple strands and cracks, defining ≃200-m-wide rupture zone.

(at the western end of the rupture, Figure 4b), and 1-m pixel Ikonos images. In areas not covered by our InSAR and Ikonos data, we based the fault model on the morphologic trace of the fault, as mapped from 3-arc sec SRTM data.

4.1. Rupture Geometry From Ikonos Images

[20] The Ikonos images available to us cover a 6-km-wide, ≃200-km-long zone over the eastern half of the rupture, from longitude 92.03° to 94.15°E, along the Kusai Hu segment of the Kunlun fault and the Kunlun Pass fault. The Xidatan segment of the Kunlun fault, on the northern front of the Burhan Budai Shan, is also partly covered, from longitude 93.75°E to 94.26°E. *Klinger et al.* [2005] provide a detailed analysis of this high-resolution data set. Here we focus on mapping the first-order geometry of the rupture, to define a simplified fault model.

[21] The 2001 rupture appears mainly linear, and tends to follow the geomorphic trace of the fault marked by cumulative scarps and features such as push-ups or pressure ridges associated with previous earthquakes (Figure 6). West and north of Kusai lake, slip partitioning occurs on two parallel strands separated by up to 2.5 km (Figure 6a) [*King et al.*, 2005]. The northern strand, along the southern front of the mountain range, accommodated mostly discontinuous downdip movement (≤1 m) during the 2001 earthquake (Figure 6a) [*Klinger et al.*, 2005]. The southern strand is mostly strike slip, cutting across alluvial fans showing evidence for left-lateral slip (Figures 6a and 6b). In our model, we took this strand to be the principal rupture trace in this area, ignoring the northern, south dipping normal strand. East of Kusai lake (east of 92.5°E), the fault is single stranded with a predominant strike-slip component of movement (Figure 6c). To this relatively simple large-scale rupture geometry, are superimposed smaller size complexities typical of earthquake surface breaks, neglected in the modeling. Figure 6 shows examples of such com-

plexities, which include transpressive and transtensive transfer zones several hundred meters in width, composed of series of push-ups (Figure 6b), pull-apart sags, en echelon step-overs and fissures (Figure 6d). No clear surface rupture was observed along the Xidatan segment of the fault, in agreement with interferogram T362 (Figure 5).

4.2. Fault Model

[22] The fault model used in the radar data inversion encompasses the entire rupture trace that we mapped, with additional segments up to 50 km long at both ends to account for possible slip at depth beyond zones where surface breaks were observed. InSAR data acquired only from descending passes of the satellite were available for this event, making it difficult to resolve trade-offs between strike slip and dip slip components of the movement, and fault dip. Given the mechanism of the earthquake and the fact that neither seismological nor geological data provide reliable constraints on the fault dip, we chose to model the fault as a vertical surface extending to a depth of 20 km. Test inversions using a fault extending deeper than 20 km indicated that virtually no slip could be resolved below this depth. We distinguish two fault sections in the model (Figure 7a): (1) a $\simeq$400-km-long section following the main Kunlun fault and the Kunlun Pass fault and (2) a $\simeq$90-km-long secondary fault at the western end of the rupture, running along the Taiyang lake fault, as mapped from the analysis of wrapped interferogram T448 (Figure 4b). The fault plane is divided into $\simeq$5-km-long $\times$ 5-km-wide patches to estimate the variation of slip along strike and with depth (Figure 7a). We chose not to include smaller fault patches in the shallow part of the fault because of the poor coherence of the interferometric phase in the vicinity of the rupture, particularly along the western part of the Kunlun fault (Figure 2), resulting in coarse resolution of the slip variability at shallow depth. The 5 km $\times$ 5 km gridded model gives a total of 372 parameters to be solved in the inversion. This number appears reasonable in view of the fault length and simple geometry and the spatial distribution of the interferometric data.

4.3. InSAR Data Decimation and Inversion

[23] The InSAR data set is composed of four unwrapped interferograms georectified to the 3-arc sec grid of the SRTM data. This represents a total of a few 10^7 data points, separated by $\simeq$90 m on the ground in coherent areas. This data set is highly correlated spatially and can be reduced without degrading the contained information. We first subsample the data by a factor of 10 in both directions, giving us a minimum posting distance of $\simeq$900 m. Data points closer than 1 km from the fault are eliminated, to take into account uncertainties on the fault location. We further decimate the number of data points by adjusting the local density of sampling to the local gradient of LOS displacement throughout each scene. Between two neighboring points, a minimum LOS displacement difference of 2 cm and a maximum distance of 7 km are required. In the inversion, each point is weighted in proportion to the number of points it represents in the original data set. Given the coseismic displacement gradient, the points are more densely distributed in the near field than in the far field in the decimated data set (Figure 8). This procedure reduces the data set to a more manageable number of points of about 5×10^3, preserving the high resolution of InSAR in areas of good coherence and large displacement gradient (Figure 8).

[24] We model the surface displacement field using the analytical approach of *Okada* [1992], for a fault embedded in a homogeneous elastic half-space. At each point, the three-dimensional displacement vector is projected in the radar line of sight, taking into account the range variation of the incidence angle. Using a nonnegative least squares method, we solve for: (1) the left-lateral, strike-slip component of movement on each fault patch, (2) a bilinear ramp for each interferogram to correct for possible orbital errors, and (3) two phase constants per interferogram (one for each side of the fault). To limit oscillations of the solution, we impose some smoothing on the solution, by minimizing the first-order derivative of the slip gradient, computed by finite difference quadrature. Following the approach in *Jonsson et al.* [2002], the amount of smoothing is adjusted to obtain optimum compromise between the average slip gradient of the model (or roughness, in cm/km) and the misfit (L2 norm) of the solution. Figure 9 shows the trade-off curve between the model roughness and the solution misfit. Our preferred model (named m_1 in Figure 9 and presented in Figure 7a) has a roughness of about 12 cm/km. Reducing the smoothing would not decrease significantly the misfit of the solution while allowing more smoothing would rapidly increase the misfit.

4.4. Variable Slip Model

[25] Our solution (Figures 7 and 10) shows that the rupture extends from longitude 90.2°E to 94.5°E, and includes distinct sections of moment release along the Taiyang lake fault (TLF), the Kusai Hu segment of the main Kunlun fault (MKF), and the Kunlun Pass fault (KPF). Four of these sections have resolved slip exceeding 5 m.

[26] Along the TLF, in the epicentral area, we observe one main section of large moment release, contributing to 20% of the total moment (Figure 10b). Below 10 km, the slip distribution is rather uniform up to the junction with the MKF, with slip values reaching 3 m. Above 10 km, the slip distribution defines two maxima of different magnitude on either side of the Taiyang lake. The estimated slip reaches 5 m along the Heituo strike-slip fault and is less than 2 m along the SW-NE normal fault east of Taiyang lake (Figure 10b). Three sections of large moment release, accounting for 65% of the total moment release, can be distinguished along the MKF and are associated with three shallow slip maxima of 6.5 m, 8 m, and 8 m, from west to east, respectively. Along the KPF, a 40-km-long section with two slip maxima of 3.5 m at the surface terminates the rupture to the east. As at the western end of the rupture, slip at depth appears to be higher along the KPF than along the MKF, with values of up to 4 m observed at depths between 15 and 20 km.

[27] The moment computed from the solution (7.1×10^{20} Nm) is higher than the seismological estimates (Harvard CMT 5.8×10^{20} N m). As stated before, InSAR data contain interseismic and postseismic deformation, which may contribute to the geodetic moment. The slip distribution solution obtained from inversion of GPS data including coseismic deformation and 4 months of postseismic deformation, provides a moment estimate of 8×10^{20} N m [*Wang et al.*, 2003], consistent with the moment of our solution.

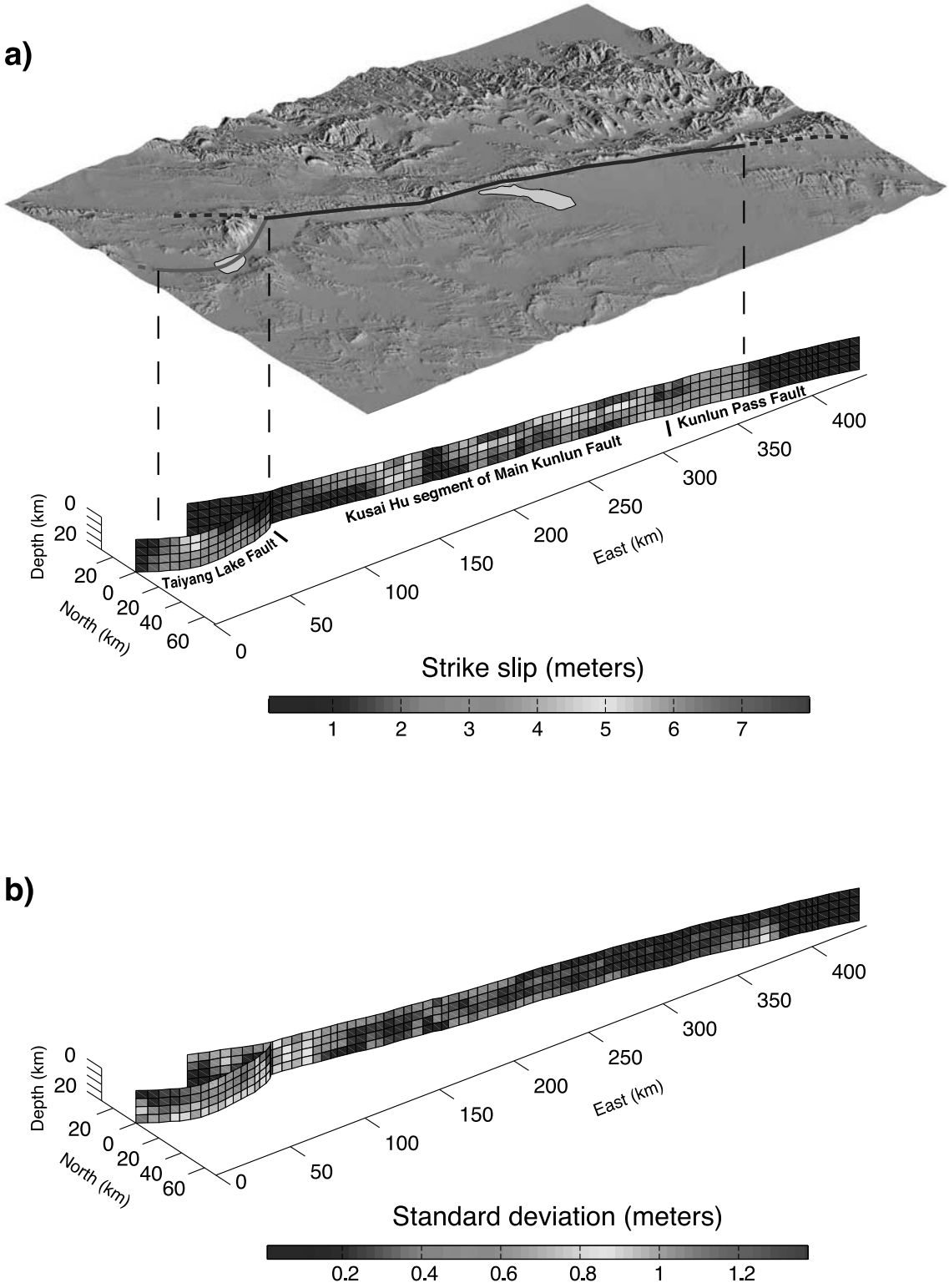

Figure 7. (a) (top) The 3-D shaded view of topography in 2001 Kokoxili earthquake area, from 3-arc sec SRTM data. Blue and red lines outline modeled fault trace used for inversion along Kunlun and Kunlun Pass faults and Taiyang lake fault, respectively. (bottom) Vertical, 5 km × 5 km gridded fault model and estimated strike-slip distribution of our preferred model (m_1 on Figure 9), obtained by averaging 50 solutions from inversion of data sets with correlated noise (see text for details). (b) Associated standard deviation distribution. See color version of this figure at back of this issue.

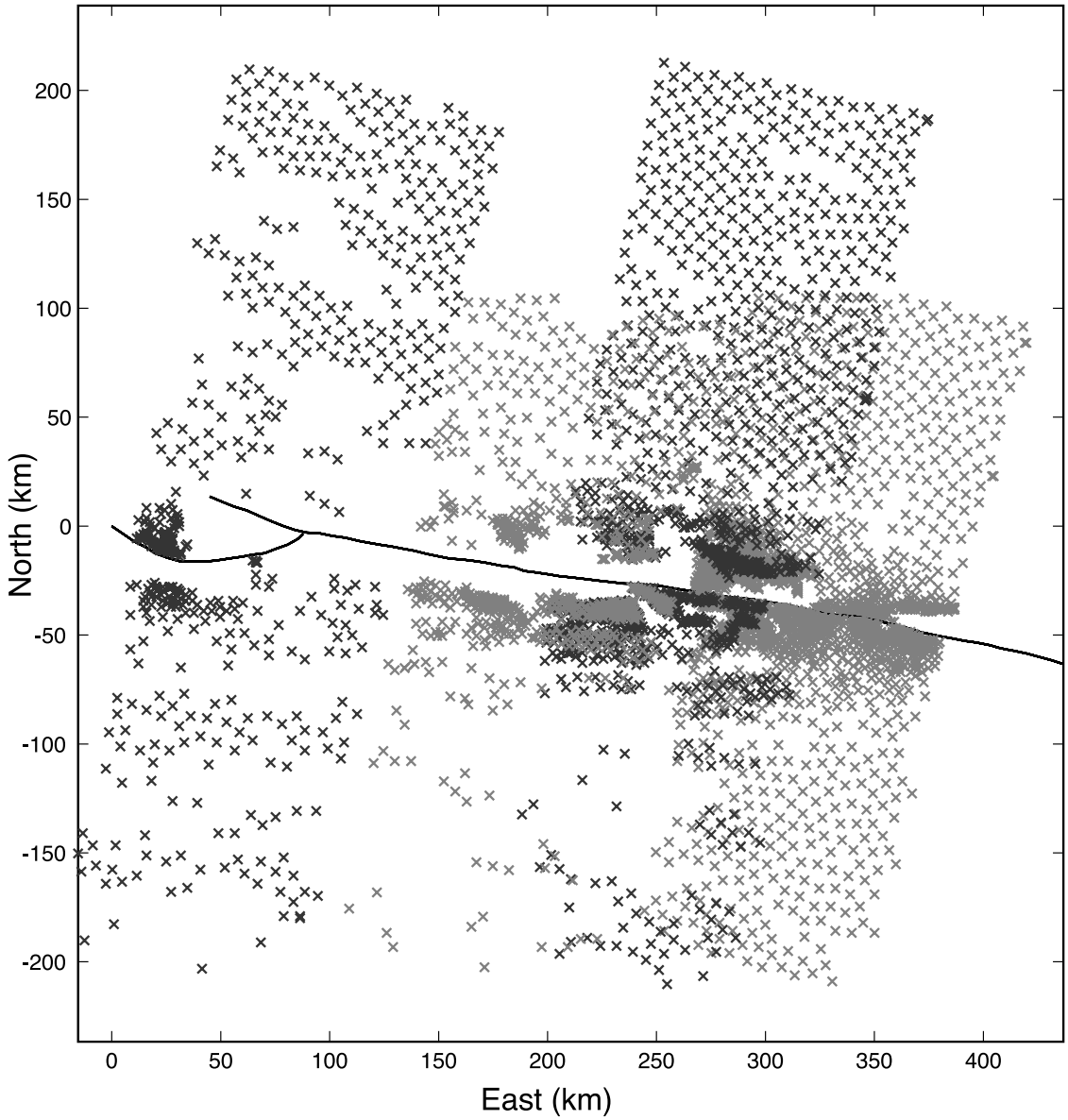

Figure 8. Map showing distribution of InSAR data points in 2001 event area after data decimation. Sampling density is adjusted to LOS displacement gradient in the rupture vicinity (see text for details on decimation procedure). Black and grey crosses locate selected points on interferograms of Figure 2. Black lines outline surface trace of fault model. Note poor data sampling on western interferograms in rupture zone due to poor phase coherence.

[28] Figure 11 shows a comparison between our preferred model and the observed surface displacement field. The residuals between the InSAR data and the model are less than 10 cm almost everywhere, with the largest values observed near the fault trace. The fact that we use a vertical fault and do not solve for the downdip component of slip explains in part the largest residuals in the vicinity of the fault. SE and SSW dipping normal throws (up to 1 m) are clear on the eastern part of the TLF and in the central part of the MKF (referred as segments 2 and 4 on Figure 10a), respectively. Given the direction of the satellite line of sight, this results in underestimating the horizontal slip values along these two segments in our model. Along the central part of the MKF for example, 8 m of pure left-lateral slip projects into $\simeq$3 m of LOS displacement, similarly as 10 m of left-lateral slip combined with 1 m of SSW dipping normal throw.

[29] The model resolution mostly depends on the InSAR data spatial distribution and errors, and on the level of smoothing imposed to the solution. The main source of errors in InSAR data is the phase propagation delay through the troposphere [e.g., *Goldstein*, 1995]. Our experience with observation of interferograms with no or negligible signal in Tibet indicates that the residual phase delay is generally less than $\simeq$2 cycles, leading to an error of $\simeq$56 mm in line of sight displacement. The spatial distribution of the areas of coherent phase in the interferograms is also a key factor for the resolution of our model. In places where measurements can be made close to the faults, the constraints on the slip solution at shallow depth are clearly stronger than on fault

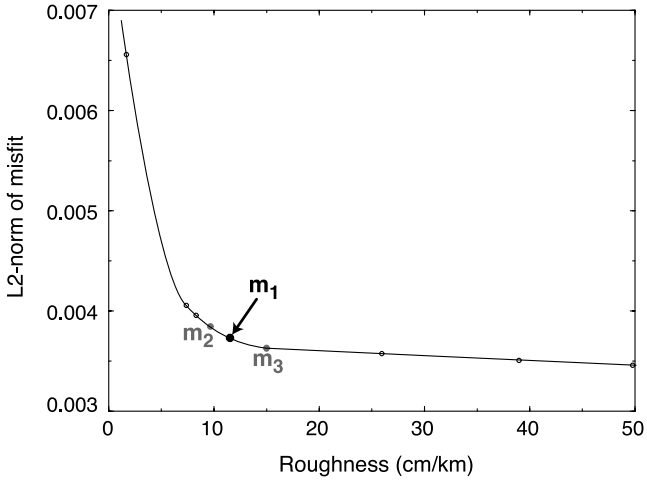

Figure 9. L2 norm of least squares inversion misfit plotted as a function of solution roughness (average slip gradient). Note trade-off between L2 norm and roughness. Arrow points to parameters corresponding to our preferred model (m_1). Surface slip distribution curves corresponding to models m_1, m_2 and m_3 are shown in Figure 10b.

sections distant from coherent phase areas (Figures 7 and 8). We performed a complete assessment of the combined influence of tropospheric noise and data spatial distribution on our fault slip solution, using a Monte Carlo approach as described by *Crampé et al.* [2000] and *Wright et al.* [2003]. We first generate a series of fifty synthetic maps of spatially correlated noise, matching the one-dimensional power spectra of tropospheric signal in typical interferograms of Tibet. These noise maps are added to the observed InSAR data to construct fifty noisy data sets that are subsequently inverted using the optimum smoothing coefficient determined above (Figure 9). The synthetic data have the same spatial distribution as the real data set. The mean slip of the fifty solutions and the associated standard deviation are shown for each fault patch in Figure 7. Their along-strike distribution in the upper 5 km of the fault is shown in Figures 10b and 10c for three different solutions. The standard deviation values for each patch provide a robust assessment of the errors on the mean solution, given the data spatial distribution, our model assumptions and inversion procedure. The largest errors (up to 1.3 m) are observed in the junction area between the TLF and the MKF (Figure 7b), where data points are sparse (Figure 8). Errors above 0.7 m observed

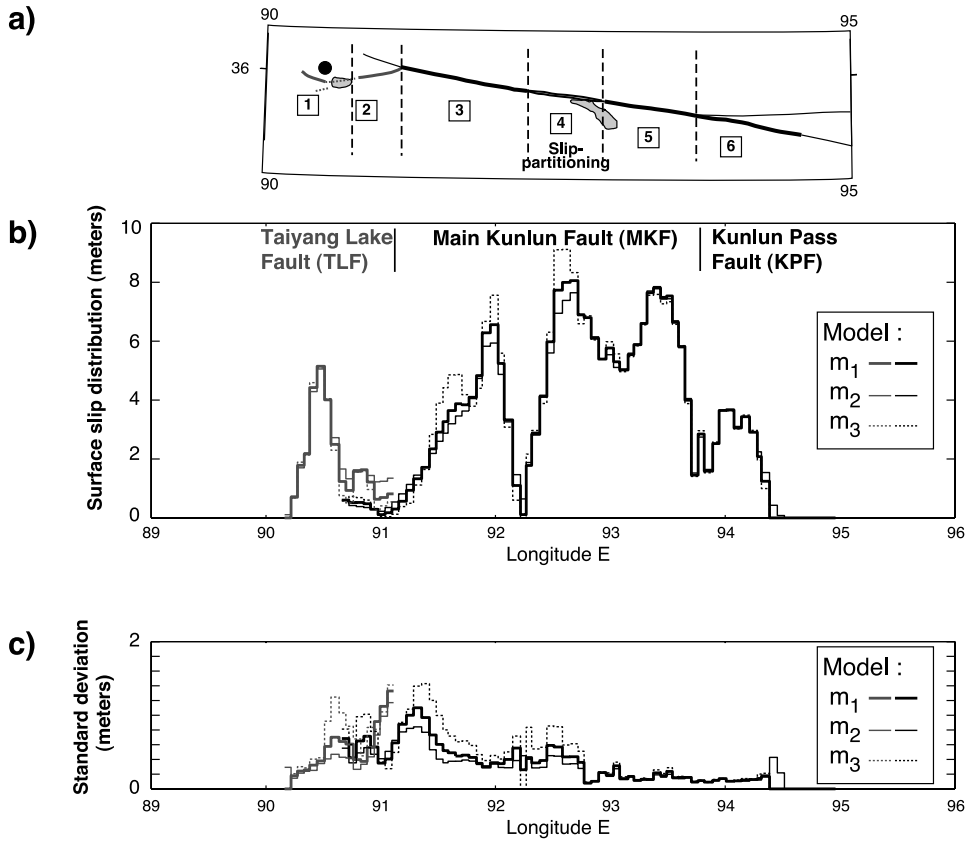

Figure 10. (a) First-order segmentation of Kunlun fault system along 2001 rupture from this study, *Van der Woerd et al.* [2002b], and *Xu et al.* [2002]. Minor normal component of slip was observed in the field along segment 2 (east of Taiyang lake) and segment 4 (where slip partitioning occurred, see Figure 6a) [*Klinger et al.*, 2005]. (b) Along-strike slip distribution from upper 5 km (0–5 km depth) of slip models m_1, m_2, and m_3 in Figure 9, with same scale as in Figure 10a. Heavy lines show slip along MKF and KPF (black) and TLF (grey) from preferred model m_1. Thin lines show slip distribution from models m_2 (solid) and m_3 (dashed). Note correspondence between sections of moment release along 2001 rupture and fault segments in Figure 10a. (c) Error on variable slip solution of Figure 10b determined using Monte Carlo approach (see text). Color code is same as in Figure 10b.

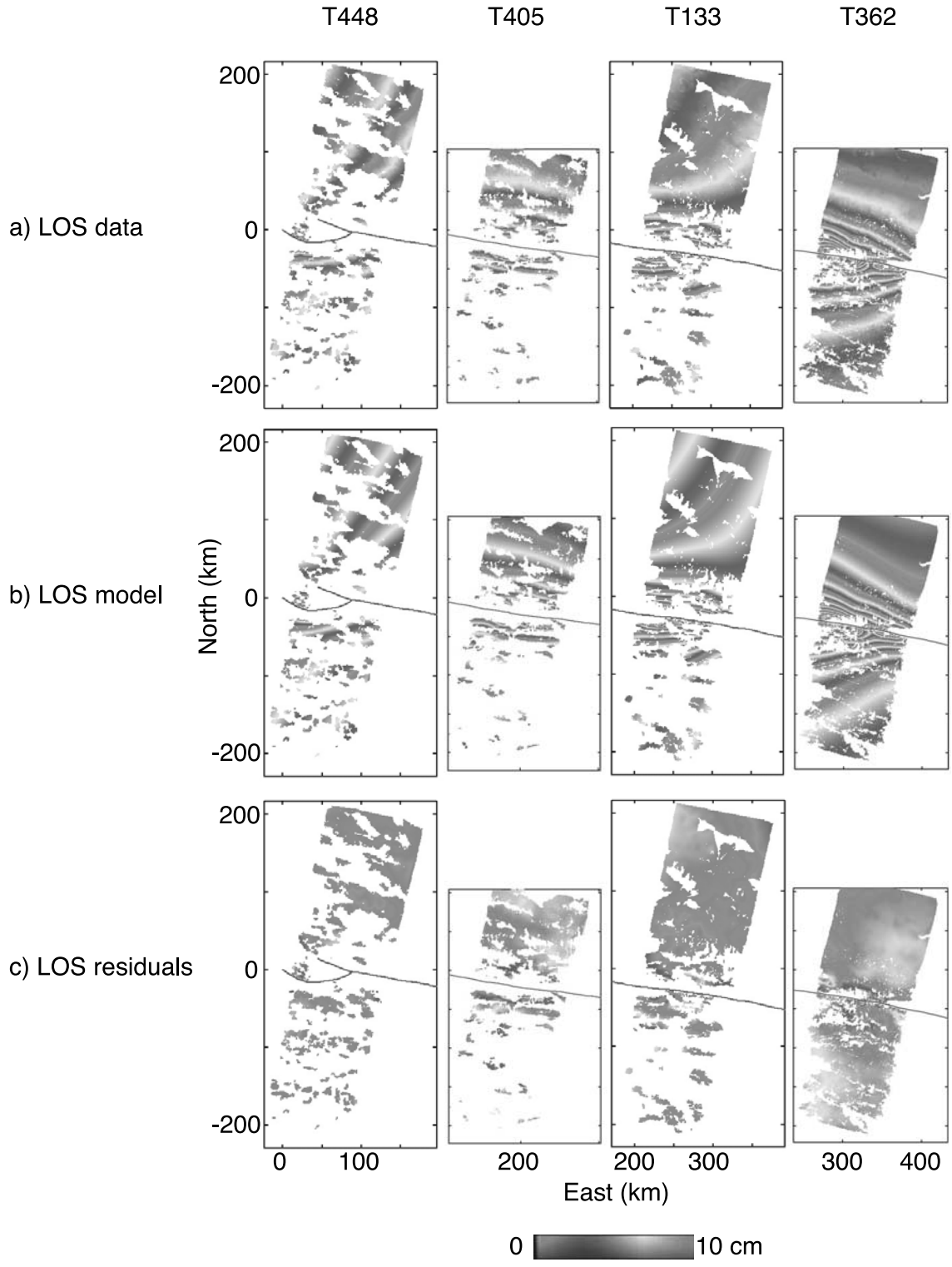

Figure 11. (a) InSAR data, (b) model predictions, and (c) residuals after subtracting model predictions from data for interferograms T448, T405, T133, and T362. One color cycle represents 10 cm of LOS. Residuals are below 10 cm almost everywhere. See color version of this figure at back of this issue.

below 15 km along the eastern part of the TLF might be due both to the sparse data distribution in the far field and to the oversimplification of the fault model in this region. In all other parts of the fault however, errors remain below 0.6 m, in particular along the sections of the fault where most of the moment was released (Figures 10b and 10c). Note that an ambiguity error of one cycle on a small patch of coherent phase, and a tropospheric delay of 2π covering the same area would result in a similar error on the slip solution. Therefore the influence of possible phase ambiguity errors on our model is implicity assessed in the procedure described above.

[30] Comparing solutions obtained with various levels of smoothing also helps identify the sections of the fault where model slip values are best constrained (Figures 10b and 10c). Model 1 (m_1) provides our preferred compromise between smoothness and misfit and corresponds to an average slip gradient of 12 cm/km. Models 2 and 3 (m_2 and m_3) involve more and less smoothing, respectively (Figure 9). Along sections of the fault where the distribution of data points at the surface brackets the fault closely (Figure 8), the shallow slip and its standard deviation (below 0.4 m, Figures 10b and 10c) are not affected by the degree of smoothing and slip estimates are reliable. This is quite clear west of Taiyang lake and along the eastern half of the fault, east of Kusai lake (Figure 10b). In areas where data points become sparse in the vicinity of the fault, the solution is less constrained and the degree of smoothing has more influence on the shallow slip solution. For example, the magnitudes of the two slip maxima observed west of Kusai lake along the MKF vary as a function of the smoothing factor and are consequently less constrained (±1 m, Figure 10b).

4.5. Discussion

[31] It is interesting to compare our slip model for the shallowest patches, between 0 and 5 km (Figure 10b), with the surface slip distributions obtained from various field campaigns and from high-resolution satellite imagery analysis. Our InSAR model yields a maximum slip associated with the 2001 Kokoxili earthquake of about 8 m, along two contiguous sections on both sides of Kusai lake, about 200 and 250 km east of the epicenter (Figure 10b). This maximum value is half that (≃16 m) reported by *Lin et al.* [2002], which was based on a preliminary field survey, but it is consistent with the more extensive field studies of the surface rupture conducted since [*Xu et al.*, 2002, 2003; *Klinger et al.*, 2005]. Slip measurements from the latter fieldwork show a slip distribution comparable to that in our model along the TLF and KPF. However, *Xu et al.* [2002] identify a single maximum of slip of 7.6 m located east of Kusai lake along the MKF, whereas our slip distribution bears three maxima along the MKF (Figure 10b). The existence of these three maxima is supported both by offsets measurements made on Ikonos and Quick Bird images acquired after the 2001 event [*Klinger et al.*, 2005], and by offset maps derived from optical correlation of SPOT images acquired before and after the event [*Klinger et al.*, 2004].

[32] A striking feature of our slip distribution model is the relatively shallow slip (Figure 7). In this respect, the 2001 M_w = 7.8 Kokoxili event is quite similar to the 1997 M_w = 7.6 Manyi event at the southwestern end of the Kunlun fault system [*Crampé et al.*, 2000] (Figure 1a). Slip appears to be mostly concentrated within the upper 10 km of the fault, along the MKF in particular, with the largest slip occurring within the upper 5 km. This slip distribution and the overall consistency between the 0–5 km average slip and the surface offsets measurements made on high-resolution optical images [*Klinger et al.*, 2005] may suggest that there is no significant slip deficiency in the uppermost few kilometers of the crust. This contrasts with observations made in other cases [*Simons et al.*, 2002; *Fialko et al.*, 2005]. However, the 5 km vertical dimension of the fault patches in our model limits our capability of detecting a potential peak of slip around 5 km depth.

[33] As observed in models derived from seismological data [*Antolik et al.*, 2004], our solution shows significant slip below 10 km near the extremities of the rupture. Slip values of up to 3 ± 1.1 m and 4 ± 0.6 m are estimated at depth along the TLF and KPF, respectively (Figure 7). Along the TLF, where the 2001 rupture initiated, slip on the deeper section of the fault may have developed before the rupture started on the MKF, gradually building the necessary stress to permit slip transfer to the MKF and subsequently the generation of the main rupture event (Figure 7a). Along the KPF, a fault asperity may be responsible for the termination of the rupture. Accumulated stress along this fault section may not have reached the required threshold to allow the rupture to continue farther east, but was partially released by slip on the deeper section of the fault. *Antolik et al.* [2004] advocate a dynamic effect due to the rapid decrease of the rupture velocity east of the largest slip patch along the MKF, to explain the occurrence of slip on the deep section of the fault near its eastern end.

[34] A characteristic of our model is the significant along-strike variability of slip at shallow depth (Figures 7a and 10b). Such variations could be due to different slip histories during past earthquakes or varying frictional parameters along the fault. Our slip distribution model at shallow depth features six distinct sections (Figure 10b). These six sections, modeled with no constraints on slip at the surface, remarkably match the six subsegments of the Kunlun fault system, as defined from the surface morphology of the fault (Figure 10a). For example, the central zone of higher slip along the MKF, west of Kusai lake, corresponds to the well identified subsegment of the fault where slip is partitioned into two parallel strands [*Van der Woerd et al.*, 2002a; *King et al.*, 2005; *Klinger et al.*, 2004]. The near zero drop in slip at ≃92.25°E corresponds to the western end of the slip-partitioning zone. This strong correlation between rupture and fault geometry suggests that the long-term fault segmentation played a leading role in controlling rupture propagation, as also noted in other earthquake studies of major strike-slip faults [e.g., *Barka and Kadinsky-Cade*, 1988; *Çakir et al.*, 2003].

5. Summary and Conclusion

[35] Using four ERS interferograms covering an area of about 400 km × 400 km around the rupture zone and high-resolution Ikonos images, we have mapped the surface displacements associated with the 2001 Kokoxili earthquake and estimated the slip distribution along the fault plane.

[36] The radar data show that in the epicentral area, the rupture was continuous from the secondary Heituo fault to the main Kunlun fault, cutting across the Buka Daban Feng pull-apart in between these two strike-slip faults. The rupture transferred to the Kusai Hu segment of the main Kunlun fault and propagated for more than 300 km farther east, ending along the Kunlun Pass fault. The 2001 event failed to rupture the Xidatan segment of the main Kunlun fault, which splays off the Kunlun Pass fault to the north. The left-lateral slip solution obtained by least squares inversion of InSAR data, although of variable resolution

along the fault strike and with depth, indicates that slip mostly occurred within the upper 10 km of the fault plane. However, large values of slip may exist below this depth near both ends of the rupture: along the Taiyang Lake fault to the west, probably contributing to the transfer of stress to the main Kunlun Fault, and along the Kunlun Pass fault to the east. Despite the remarkably linear geometry of the main Kunlun fault, the horizontal slip solution revealed a highly variable distribution of slip along the fault strike. The envelope of the shallow slip distribution curve along the main Kunlun fault has a bell shape reaching a slip maximum of about 8 m in the center. However, the actual distribution curve shows downward incursions where the slip abruptly drops. The points of lower slip along the fault correspond to complexities in the fault geometry, and bracket smooth subsegments of the fault system along which the stress is preferably released.

[37] InSAR data thus provide a synoptic view of the 2001 displacement field, consistent with independent local observations of the rupture and offset measurements from fieldwork and analysis of high-resolution satellite images. Coverage of the radar data extends along the entire fault length, and displacement is measured up to a distance of 200 km from the fault, providing constraints on the depth extent of the rupture.

[38] The Kokoxili earthquake occurred along a critical stretch of the Kunlun fault system. Its epicenter lies about 250 km northeast of the epicenter of the 1997, M_w = 7.6, Manyi event, and the rupture ended about 150 km west of the epicenter of a M_w = 7.1 event that occurred in 1963 (Figure 1a). Clearly, the unruptured fault segments between these three rupture zones are under increased stress and may be the loci of large earthquakes in the near future. In particular, the Xidatan segment of the Kunlun fault, east of the Kusai Hu segment, has not been activated in the past few hundred years [*Van der Woerd et al.*, 1998, 2002a, 2002b] and stands out as a likely site for a future event. The sequence of earthquakes along the Kunlun fault system since 1960 does not seem to follow a unidirectional propagation pattern, as observed along the North Anatolian fault for example [e.g., *Stein et al.*, 1997]. This supports the idea that the geometric complexities segmenting the fault, rather than the local stress change produced by successive events, are controlling the generation of earthquakes in a gradually increasing regional stress field.

[39] **Acknowledgments.** This work was supported by the U.S. National Science Foundation (EAR-0125688). C. Lasserre was also partly supported by a Lavoisier fellowship (Ministère des Affaires Etrangères, France) while at UCLA. ERS data were provided by the European Space Agency under a category 1 proposal. Ikonos images were acquired through the NASA Data Purchase Program (contract NAF 13-98048) and special funding from Institut National des Sciences de l'Univers, CNRS (France). We also thank two anonymous reviewers and the Associate Editor whose comments improved the manuscript.

References

Antolik, M., R. E. Abercrombie, and G. Ekström (2004), The 14 November, 2001 Kokoxili (Kunlunshan), Tibet, earthquake: Rupture transfer through a large extensional step-over, *Bull. Seismol. Soc. Am.*, *94*(4), 1173–1194.

Barka, A., and K. Kadinsky-Cade (1988), Strike-slip fault geometry in Turkey and its influence on earthquake activity, *Tectonics*, *7*, 663–684.

Bouchon, M., and M. Vallée (2003), Observation of long supershear rupture during the magnitude 8.1 Kunlunshan earthquake, *Science*, *301*, 824–826.

Bowman, D., G. King, and P. Tapponnier (2003), Slip partitioning by elastoplastic propagation of oblique slip at depth, *Science*, *300*, 1121–1123.

Çakir, Z., J-.B. de Chabalier, R. Armijo, B. Meyer, A. Barka, and G. Peltzer (2003), Coseismic and early post-seismic slip associated with the 1999 Izmit earthquake (Turkey), from SAR interferometry and tectonic field observations, *Geophys. J. Int.*, *155*, 93–110.

Crampé, F., G. Peltzer, F. Pollitz, and R. Burgmann (2000), The magnitude M_w = 7.6 Manyi (Tibet) earthquake: Co-seismic slip solution and post-seismic relaxation processes from ERS InSAR data, *Eos Trans. AGU*, *81*(48), Fall Meet. Suppl., Abstract T72B-06.

Farr, T. G., and M. Kobrick (2000), Shuttle Radar Topography Mission produces a wealth of data, *Eos Trans. AGU*, *81*(48), 583, 585.

Fialko, Y., D. Sandwell, M. Simons, and P. Rosen (2005), Three-dimensional deformation caused by the Bam, Iran, earthquake and the origin of shallow slip deficit, *Nature*, *435*, 295–299, doi:10.1038/nature03425.

Fitch, T. J. (1970), Earthquake mechanisms in the Himalayan, Burmese, and Adaman regions and continental tectonics in central Asia, *J. Geophys. Res.*, *75*, 2699–2709.

Freymueller, J., and Q. Wang (2003), Asymmetric postseismic deformation following the 2001 Kokoxili earthquake requires heterogeneity in material properties, *Geophys. Res. Abstr.* [CD-ROM], *5*, Abstract 13882.

Goldstein, R. (1995), Atmospheric limitations to repeat-track radar interferometry, *Geophys. Res. Lett.*, *22*, 2517–2520.

Gu, G., T. Lin, and Z. Shi (1989), *Catalogue of Chinese Earthquakes (1831 BC–1969 AD)*, Science Press, Beijing.

Harris, R. A., and S. M. Day (1993), Dynamics of fault interaction: Parallel strike-slip faults, *J. Geophys. Res.*, *98*, 4461–4472.

Jia, Y., H. Dai, and X. Su (1988), Tuosuo Lake earthquake fault in Qinghai province, in *Research on Earthquake Faults in China*, pp. 66–71, Xinjiang Seismol. Bur., Xinjiang Press, Xinjiang, China.

Jonsson, S., H. Zebker, P. Segall, and F. Amelung (2002), Fault slip distribution of the 1999 M_w 7.1 Hector Mine, California, earthquake, estimated from satellite radar and GPS measurements, *Bull. Seismol. Soc. Am.*, *92*(4), 1377–1389.

Kidd, W., and P. Molnar (1988), Quaternary and active faulting observed on the 1 985 Academia Sinica-Royal Geotraverse of Tibet, *Philos. Trans. R. Soc. London, Ser. A*, *327*, 337–363.

King, G., Y. Klinger, D. Bowman, and P. Tapponnier (2005), Slip partitioned surface breaks for the M_w 7.8 2001 Kokoxili earthquake, China, *Bull. Seismol. Soc. Am.*, *95*(2), 731–738.

Klinger, Y., R. Michel, C. Lasserre, X. Xu, P. Tapponnier, J. Van der Woerd, and G. Peltzer (2004), Surface rupture of the Nov. 14th 2001 Kokoxili earthquake (M_w 7.8) imaged from space, paper presented at 3rd International Conference on Continental Earthquakes, China Earthquake Admin., Beijing.

Klinger, Y., X. Xu, P. Tapponnier, J. Van der Woerd, C. Lasserre, and G. King (2005), High-resolution satellite imagery mapping the rupture and slip distribution of the M_w = 7.8, November 14, 2001 Kokoxili earthquake (Kunlun, Tibet, China), *Bull. Seismol. Soc. Am.*, *95*(5), 1970–1987.

Li, L., and Y. Jia (1981), Characteristics of the deformation band of the 1937 Tuosuohu earthquake (M = 7.5) in Qinghai, *Northwest. Seismol. J.*, *3*(3), 61–65.

Li, H., J. Van der Woerd, P. Tapponnier, Y. Klinger, X. Qi, J. Yang, and Y. Zhu (2005), Slip rate on the Kunlun fault at Hongshui Gou, and recurrence time of great events comparable to the 14/11/2001, M_w = 7.9 Kokoxili earthquake, *Earth. Planet. Sci. Lett.*, *237*, 285–299.

Lin, A., B. Fu, J. Guo, Q. Zeng, G. Dang, W. He, and Y. Zhao (2002), Co-seismic strike-slip and rupture length produced by the 2001 M_s8.1 central Kunlun earthquake, *Science*, *296*, 2015–2017.

Massonnet, D., M. Rossi, C. Carmona, F. Adragna, G. Peltzer, K. Feigl, and T. Rabaute (1993), The displacement field of the Landers earthquake mapped by radar interferometry, *Nature*, *364*, 138–142.

Molnar, P., and H. Lyon-Caen (1989), Fault plane solutions of eathquakes and active tectonics of the Tibetan Plateau and its margins, *Geophys. J. Int.*, *99*, 123–153.

Okada, Y. (1992), Internal deformation due to shear and tensile faults in a half-space, *Bull. Seismol. Soc. Am.*, *82*(2), 1018–1040.

Peltzer, G., F. Crampé, and G. King (1999), Evidence of nonlinear elasticity of the crust from the M_w = 7.6 Manyi (Tibet) earthquake, *Science*, *286*, 272–276.

Rivera, L., J. Van der Woerd, A. Tocheport, Y. Klinger, and C. Lasserre (2003), The Kokoxili, November 14, 2001, earthquake: History and geometry of the rupture from teleseismic data and field observations, *Geophys. Res. Abstr.* [CD-ROM], *5*, Abstract 10910.

Rosen, P., S. Hensley, I. Joughin, F. Li, S. Madsen, E. Rodriguez, and R. Goldstein (2000), Synthetic aperture radar interferometry - invited paper, *Proc. IEEE*, *88*(3), 333–382.

Rosen, P. A., S. Hensley, and G. Peltzer (2004), Updated Repeat Orbit Interferometry package released, *Eos Trans. AGU*, *85*(5), 47.

Shen, Z.-K., Y. Zeng, M. Wang, Q. Wang, Q.-L. Wang, Y. Wan, W. Gan, and Z. Zhang (2003), Postseismic deformation modeling of the 2001 Kokoxili earthquake, western China, in *Geophys. Res. Abstr.* [CD-ROM], *5*, Abstract 07840.

Simons, M., Y. Fialko, and L. Rivera (2002), Coseismic deformation from the 1999 M_w 7.1 Hector Mine, California earthquake as inferred from InSAR and GPS observations, *Bull. Seismol. Soc. Am.*, *92*(4), 1390–1402.

Stein, R., A. Barka, and J. Dieterich (1997), Progressive failure on the north Anatolian fault since 1939 by earthquake stress triggering, *Geophys. J. Int.*, *128*, 594–604.

Tapponnier, P., and P. Molnar (1977), Active faulting and tectonics in China, *J. Geophys. Res.*, *82*, 2905–2930.

Tapponnier, P., Z. Xu, F. Roger, B. Meyer, N. Arnaud, G. Wittlinger, and J. Yang (2001), Oblique stepwise rise and growth of the Tibet Plateau, *Science*, *294*, 1671–1678.

Vallée, M., M. Bouchon, and J. Guilbert (2003), The Kokoxili earthquake as seen by the conjoint use of body and surface waves, *Geophys. Res. Abstr.*, [CD-ROM], *5*, Abstract 10142.

Van der Woerd, J., F. J. Ryerson, P. Tapponnier, Y. Gaudemer, R. Finkel, A. S. Mériaux, M. Caffee, G. Zhao, and Q. He (1998), Holocene left-slip rate determined by cosmogenic surface dating on the Xidatan segment of the Kunlun fault (Qinghai, China), *Geology*, *26*, 695–698.

Van der Woerd, J., et al. (2000), Uniform slip-rate along the Kunlun fault: Implications for seismic behaviour and large-scale tectonics, *Geophys. Res. Lett.*, *27*, 2353–2356.

Van der Woerd, J., A.-S. Mériaux, Y. Klinger, F. Ryerson, Y. Gaudemer, and P. Tapponnier (2002a), The 14 November 2001, M_w = 7.8 Kokoxili earthquake in northern Tibet (Qinghai province, China), *Seismol. Res. Lett.*, *73*(2), 125–135.

Van der Woerd, J., P. Tapponnier, F. Ryerson, A.-S. Mériaux, B. Meyer, Y. Gaudemer, R. Finkel, M. Caffee, G. Zhao, and Z. Xu (2002b), Uniform Post-glacial slip-rate along the central 600 km of the Kunlun fault (Tibet), from ^{26}Al,^{10}Be and ^{14}C dating of riser offsets, and climatic origin of the regional morphology, *Geophys. J. Int.*, *148*, 356–388.

Van der Woerd, J., Y. Klinger, P. Tapponnier, X. Xu, W. Chen, W. Ma, and G. King (2003), Coseismic offsets and style of surface ruptures of the 14 November 2001 M_w = 7.8 Kokoxii earthquake (northern Tibet), *Geophys. Res. Abstr.*, [CD-ROM], *5*, Abstract 11151.

Velasco, A. A., C. J. Ammon, and S. L. Beck (2000), Broadband source modeling of the November 8, 1997, Tibet (M_w = 7.5) earthquake and its tectonic implications, *J. Geophys. Res.*, *105*, 28,065–28,080.

Wang, M., Z.-K. Shen, J. Chen, Z. Zhang, Q.-L. Wang, and W. Gan (2003), Slip distribution of the 2001 M_w 7.8 Kokoxili earthquake, western China, *Geophys. Res. Abstr.*, [CD-ROM], *5*, Abstract 05549.

Wang, Q., et al. (2001), Present-day deformation in China constrained by global positioning system measurements, *Science*, *294*, 574–575.

Wright, T. J., Z. Lu, and C. Wicks (2003), Source model for the M_w 6.7, 23 October 2002, Nenana Mountain earthquake (Alaska) from InSAR, *Geophys. Res. Lett.*, *30*(18), 1974, doi:10.1029/2003GL018014.

Xu, X., W. Chen, W. Ma, G. Yu, and G. Chen (2002), Surface rupture of the Kunlunshan earthquake (M_s8.1), northern Tibetan Plateau, China, *Seism. Res. Lett.*, *73*(6), 884–892.

Xu, X., W. Chen, W. Ma, J. Van der Woerd, Y. Klinger, P. Tapponnier, G. King, R. Zhao, and J. Li (2003), Reevaluation of co-seismic strike-slip and surface rupture length of the 2001 Kunlunshan earthquake, northern Tibetan Plateau, China, *Geophys. Res. Abstr.* [CD-ROM], *5*, Abstract 03870.

Zebker, H., and J. Villasenor (1992), Decorrelation in interferometric radar echoes, *IEEE Trans. Geosci. Remote Sens.*, *30*, 950–959.

Zebker, H., P. Rosen, R. Goldstein, A. Gabriel, and C. Werner (1994), On the derivation of coseismic displacement-fields using differential radar interferometry: The Landers earthquake, *J. Geophys. Res.*, *99*(B10), 19,617–19,634.

F. Crampé and G. Peltzer, Department of Earth and Space Sciences, University of California, 595 Charles E. Young Drive E., 3806 Geology building, Los Angeles, CA 90095-1567, USA. (frederic.crampe@silogic.fr; Peltzer@ess.ucla.edu)

Y. Klinger and P. Tapponnier, Institut de Physique du Globe de Paris, Laboratoire de Tectonique et Mécanique de la Lithosphère, 4, place Jussieu, F-75252 Paris Cedex 05, France. (klinger@ipgp.jussieu.fr; tappon@ipgp.jussieu.fr)

C. Lasserre, École Normale Supérieure, Laboratoire de Géologie, CNRS-UMR 8538, 24, rue Lhomond, F-75231 Paris Cedex 05, France. (lasserre@geologie.ens.fr)

J. Van der Woerd, Institut de Physique du Globe de Strasbourg, CNRS-UMR 7516, Strasbourg, France. (jerome.vanderwoerd@eost.u-strasbg.fr)

Figure 1. (a) Simplified map of Kunlun fault system. Six segments defined by *Van der Woerd et al.* [2002b] along main Kunlun fault (labeled A to F) are indicated with dashed blue vertical lines. Surface ruptures associated with 1997, $M_w = 7.6$, Manyi and 2001, $M_w = 7.8$, Kokoxili earthquakes are outlined in blue and red, respectively. Corresponding CMT focal mechanisms are in similar color. The 1937, $M = 7.5$, historical earthquake (in red [*Gu et al.*, 1989]) and $M_s > 4$ instrumental seismicity (open circles) along fault are also reported. Corresponding focal mechanisms are from *Molnar and Lyon-Caen* [1989] and USGS. Note widening of the Kunlun fault zone in a horsetail system west of the Kusai Hu segment. Inset map shows location of Kunlun fault (in red) within India-Asia collision zone. Light and dark grey boxes indicate map coverage of Figures 1a and 1b, respectively. (b) Seismotectonic map of western Kunlun fault system. The 2001 Kokoxili earthquake rupture is outlined in red. Gray and yellow circles are $M \geq 5$ events prior to the earthquake (27 March 1998 to 13 November 2001) and aftershocks (14 November 2001 to 31 December 2003), respectively. The main shock is shown in red. Locations are from Advanced National Seismic System (ANSS) catalog. Focal mechanisms from Harvard CMT catalog are plotted in similar shades and point to locations from ANSS catalog (large circles) and CMT centroids (small circles). Topography is from 3-arc sec Shuttle Topography Mission (SRTM) digital elevation data. BDF and BBS refer to Buka Daban Feng and Burhan Budai Shan summits, respectively. Black rectangles outline the location of interferograms shown in Figure 2.

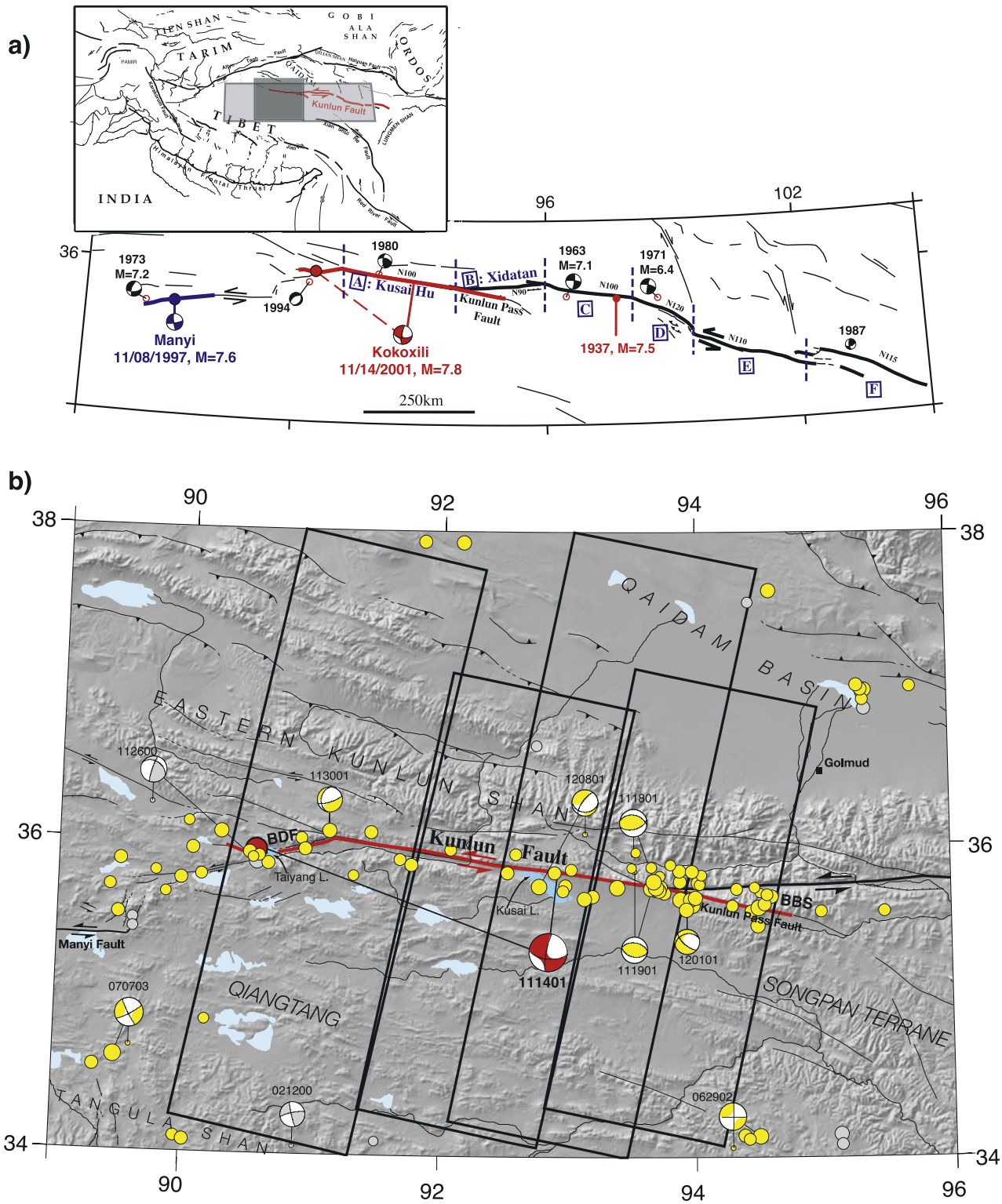
a)
TIEN SHAN
GOBI ALA SHAN
TARIM
ORDOS
QAIDAM
TIBET
INDIA
Kunlun Fault
Himalayan Frontal Thrust
Red River Fault
96
102
36
1973 M=7.2
1980
1994
A: Kusai Hu
B: Xidatan
Kunlun Pass Fault
1963 M=7.1
1971 M=6.4
C
D
E
F
1987
N100
N90
N120
N110
N115
Manyi 11/08/1997, M=7.6
Kokoxili 11/14/2001, M=7.8
1937, M=7.5
250km
b)
90
92
94
96
38
36
34
QAIDAM BASIN
EASTERN KUNLUN SHAN
Golmud
112600
113001
120801
111801
BDF
Kunlun Fault
Taiyang L.
Kusai L.
BBS
Kunlun Pass Fault
Manyi Fault
070703
111401
111901
120101
QIANGTANG
SONGPAN TERRANE
021200
062902
TANGULA SHAN

Figure 1

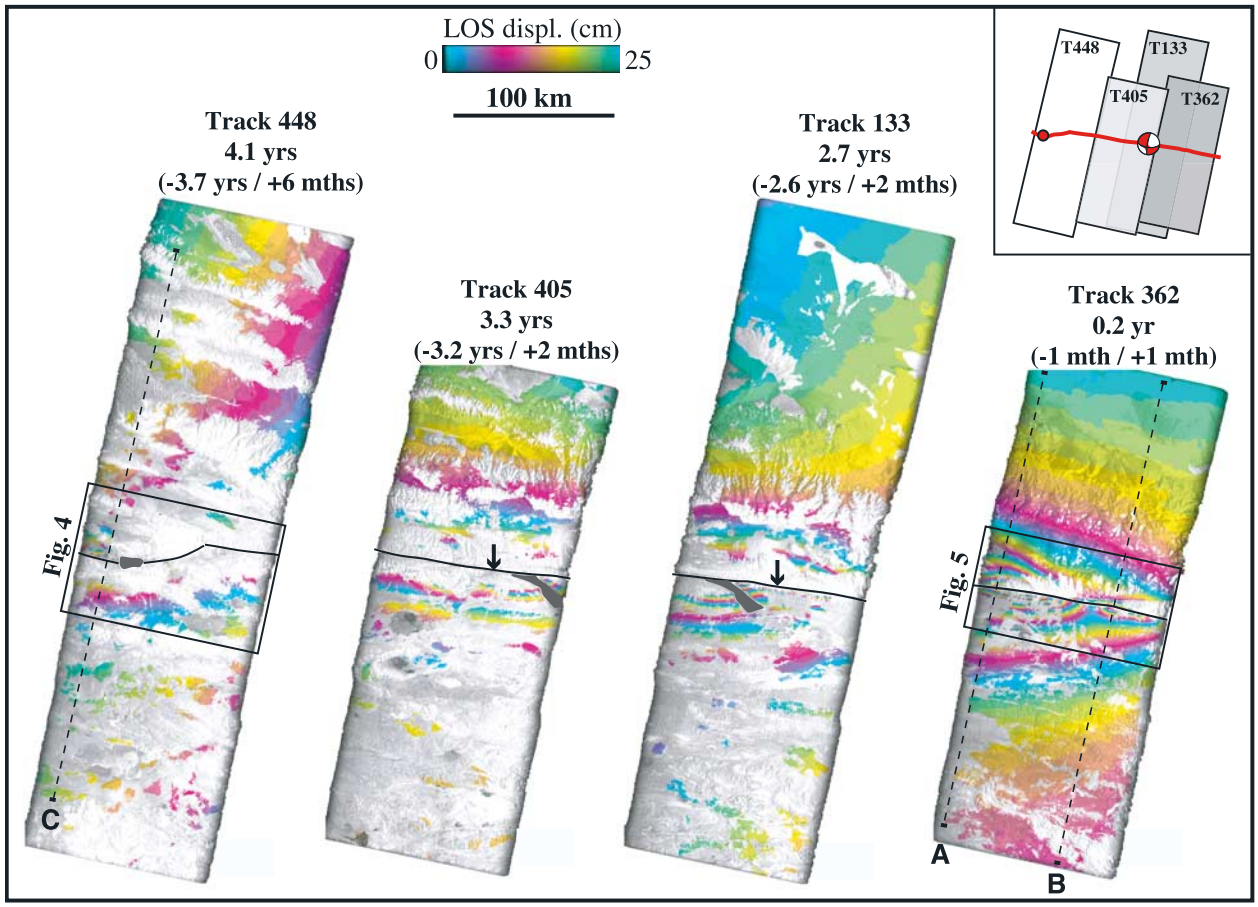

Figure 2. Interferograms showing coseismic surface displacement associated with 14 November 2001 Kokoxili earthquake. One color cycle (blue-red-yellow) represents 25 cm of ground displacement toward the satellite along radar line of sight. Grey areas are zones of low coherence that have been masked for phase unwrapping. Inset box shows locations of rupture, USGS NEIC epicenter and Harvard CMT centroid in interferograms. Time interval covered by each interferogram is indicated, with fractions of interval before and after the earthquake in parentheses (see also Table 1). Solid black line is simplified rupture trace used for modeling. Dashed lines indicate locations of profiles in Figures 3a–3c. Arrows point to location of Ikonos images shown in Figure 6. Boxes on tracks 448 and 362 indicate areas covered by Figures 4 and 5, respectively.

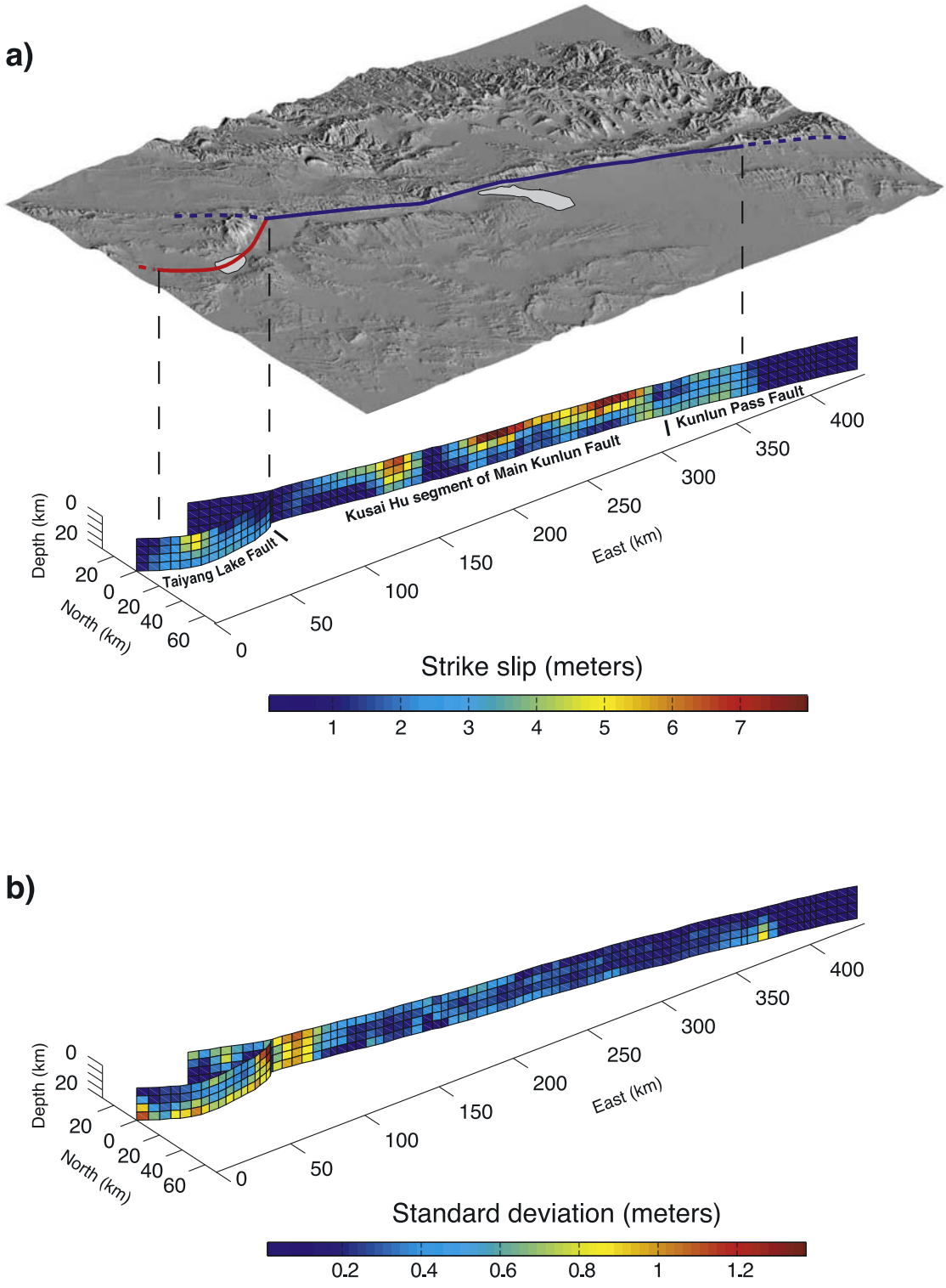

Figure 7. (a) (top) The 3-D shaded view of topography in 2001 Kokoxili earthquake area, from 3-arc sec SRTM data. Blue and red lines outline modeled fault trace used for inversion along Kunlun and Kunlun Pass faults and Taiyang lake fault, respectively. (bottom) Vertical, 5 km × 5 km gridded fault model and estimated strike-slip distribution of our preferred model (m_1 on Figure 9), obtained by averaging 50 solutions from inversion of data sets with correlated noise (see text for details). (b) Associated standard deviation distribution.

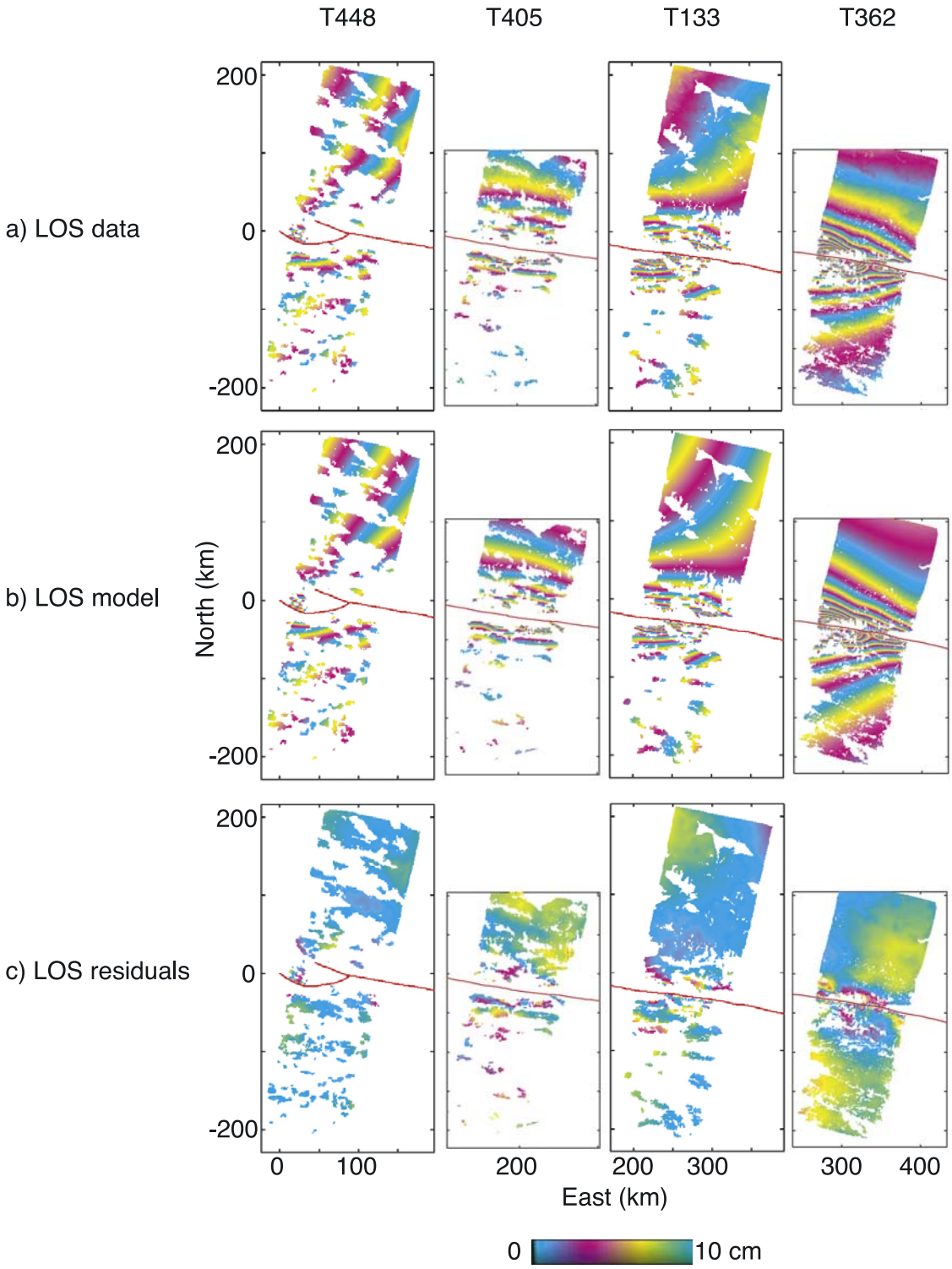

Figure 11. (a) InSAR data, (b) model predictions, and (c) residuals after subtracting model predictions from data for interferograms T448, T405, T133, and T362. One color cycle represents 10 cm of LOS. Residuals are below 10 cm almost everywhere.